Topics in Organometallic Chemistry 51

Jairton Dupont
László Kollár *Editors*

Ionic Liquids (ILs) in Organometallic Catalysis

Springer

51
Topics in Organometallic Chemistry

Aims and Scope

The series *Topics in Organometallic Chemistry* presents critical overviews of research results in organometallic chemistry. As our understanding of organometallic structure, properties and mechanisms increases, new ways are opened for the design of organometallic compounds and reactions tailored to the needs of such diverse areas as organic synthesis, medical research, biology and materials science. Thus the scope of coverage includes a broad range of topics of pure and applied organometallic chemistry, where new breakthroughs are being achieved that are of significance to a larger scientific audience.

The individual volumes of *Topics in Organometallic Chemistry* are thematic. Review articles are generally invited by the volume editors. All chapters from Topics in Organometallic Chemistry are published OnlineFirst with an individual DOI. In references, Topics in Organometallic Chemistry is abbreviated as Top Organomet Chem and cited as a journal.

More information about this series at
http://www.springer.com/series/3418

Jairton Dupont • László Kollár
Editors

Ionic Liquids (ILs) in Organometallic Catalysis

With contributions by

C.A.M. Afonso · C. Bruneau · D.A. Castillo-Molina · C. Chiappe · M. Cokoja · P. Cotugno · M.M. Dell'Anna · Q.-H. Fan · C. Fischmeister · T. Ghilardi · L.R. Graser · Y.-M. He · C. Janiak · F.E. Kühn · M. Latronico · Y. Li · P. Lignier · I.I.E. Markovits · P. Mastrorilli · A. Monopoli · C.J. Münchmeyer · A. Nacci · A. Plikhta · C.S. Pomelli · B. Rieger · A.A. Rosatella · R. Skoda-Földes · A.M. Trzeciak · N. Yan

Springer

Editors
Jairton Dupont
Institute of Chemistry - UFRGS
Porto Alegre
Brazil

László Kollár
Department of Inorganic Chemistry
Institute of Chemistry, University of Pecs
Pécs
Hungary

ISSN 1436-6002 ISSN 1616-8534 (electronic)
ISBN 978-3-662-47856-1 ISBN 978-3-662-47857-8 (eBook)
DOI 10.1007/978-3-662-47857-8

Library of Congress Control Number: 2015945264

Springer Heidelberg New York Dordrecht London

Printed on acid-free paper

Springer-Verlag GmbH Berlin Heidelberg is part of Springer Science+Business Media (www.springer.com)

Preface

The application of the right solvent in chemical reactions is always a key-point for a chemist. In addition to conventional organic solvents several alternative ones were tested. Among them ionic liquids (ILs) and especially room temperature ionic liquids (RT-ILs) play an important role due to their environmentally benign properties such as extremely low vapor pressure, chemical and thermal stability, high ionic conductivity, and good solvent properties towards both ionic and covalent compounds.

A major drive of these efforts with ionic liquid both in industry and in fundamental research is to find more environmentally friendly technologies for traditional ones in which damaging and volatile organic solvents are generally used. Ionic liquids are considered not only as promising surrogates of organic solvents in conventional text-book reactions, but also their applications show an upward tendency also in catalytic reactions.

In this book we intend to summarize the recent achievements in catalytic reactions carried out in ILs. Leading scientists worldwide accepted our invitation to contribute to this volume and write about the recent developments. Although most chapters of the book are mainly focused on the catalytic reactions of synthetic importance, where appropriate, theoretical and mechanistic aspects are included in order to help the reader understand the underlying principles. We are confident that this book will provide a comprehensive overview of topics of current interest for the non-specialist reader.

One of the fundamental issues, the homogeneous or heterogeneous catalysis in ILs, is discussed by N. Yan (chapter "The Nature of Metal Catalysts in Ionic Liquids: Homogeneous vs Heterogeneous Reactions"). The formation of nanoparticles, as well as their application in catalytic reactions (hydrogenation, coupling reactions, methanol synthesis), is discussed by Ch. Janiak (chapter "Metal Nanoparticle Synthesis in Ionic Liquids"). P. Lignier's contribution is dealing with the size control of metal nanocrystals in ILs (chapter "Size Control of Monodisperse Metal Nanocrystals in Ionic Liquids"). C. Chiappe et al. report on the structural features and properties of metal complexes in ILs with special focus on anionic speciation of metals (chapter "Structural Features and Properties of Metal

Complexes in Ionic Liquids: Application in Alkylation Reactions”). The state of the art in ionic liquid-based hydroformylation is reviewed by B. Rieger et al. (chapter “Ionic Liquids in Transition Metal-Catalyzed Hydroformylation Reactions”). The research carried out recently in the field of carbonylation of alkenes and alkynes, as well as aryl and alkenyl halides in the presence of O- and N-nucleophiles, is summarized by R. Skoda-Földes (chapter “ILs in Transition Metal-Catalysed Alkoxy- and Aminocarbonylation”). Metal-catalyzed oxidations of alcohols and sulfides are discussed by A.M. Afonso et al. (chapter “Metal-Catalyzed Oxidation of C–X (X=S, O) in Ionic Liquids”). Recent results on epoxidation of various olefins by different transition metal complexes, as wel as by metal-free compounds in ILs, are summarized by F.E. Kühn et al. (chapter “Epoxidation of Olefins with Molecular Catalysts in Ionic Liquids”). The beneficial effect of ILs in terms of activity, selectivity, and recyclability in cross-coupling reactions such as Heck, Suzuki–Miyaura, Stille, Sonogashira, Ullmann, and Negishi couplings is described by P. Mastrolilli et al. (chapter “Ionic Liquids in Palladium-Catalyzed Cross-Coupling Reactions”). The chapter of Ch. Bruneau et al. covers the catalytic olefin metathesis reactions carried out in RT-ILs (chapter “RTILs in Catalytic Olefin Metathesis Reactions”). Selected examples of polymerization and oligomerization catalyzed by transition metal complexes in ILs are presented by A.M. Trzeciak (chapter “Ionic Liquids in Transition Metal-Catalyzed Oligomerization/Polymerization”). The efficiency of transition metal-catalyzed asymmetric reactions providing precursors of pharmaceutical importance is described by Q.-H. Fan et al. (chapter “Ionic Liquids in Transition Metal-Catalyzed Enantioselective Reactions”).

We are indebted to all chapter authors for their careful work. The editors thank Elizabeth Hawkins (Springer, Chemistry Editorial) and Sujitha Shiney (Project Coordinator) for their kind cooperation in producing the present volume.

As volume editors we kindly recommend the present book entitled *Ionic Liquids in Organometallic Catalysis* to the attention of research scientists at universities or in industry, as well as graduate students.

Pécs, Hungary László Kollár
Porto Alegre, Brazil Jairton Dupont

Contents

Top Organomet Chem (2015) 51: 17–54
DOI: 10.1007/3418_2013_70

Published online: 24 January 2014

Metal Nanoparticle Synthesis in Ionic Liquids

Christoph Janiak

Abstract The synthesis of metal nanoparticles (M-NPs) in ionic liquids (ILs) can start from metals, metal salts, metal complexes, and in particular metal carbonyls and can be carried out by chemical reduction, thermolysis, photochemical, microwave irradiation, sonochemical/ultrasound-induced decomposition, electroreduction, or gas-phase synthesis, including sputtering, plasma/glow-discharge electrolysis, physical vapor deposition, or electron beam and γ-irradiation. Metal carbonyls, $M_x(CO)_y$, are commercially available and elegant precursors because the metal atoms are already in the zerovalent oxidation state for M-NPs so that no reduction is necessary. The thermal decomposition of metal complexes, including metal carbonyls in ILs by microwave irradiation, provides a fast and low-energy access to M-NPs. The reason is an excellent absorption efficiency of ILs for microwave energy due to their high ionic charge, high polarity, and high dielectric constant. Ionic liquids allow for the stabilization of M-NPs without the need of additional stabilizers, surfactants, or capping ligands because of the electrostatic and steric properties inherent to ILs. From the IL dispersion, the M-NPs can be deposited on various surfaces, including graphene derivatives and nanotubes. The formation of intermetallic MM′-nanoalloys in ILs has just begun to be explored. Examples for M(M′)-NP/IL dispersions in catalytic reactions (C–C coupling, methanol synthesis, hydrogenation) are noted.

Keywords Catalysis · Ionic liquid · Metal nanoparticle · Stabilization · Synthesis

---

C. Janiak (✉)
Institut für Anorganische Chemie und Strukturchemie, Heinrich-Heine-Universität Düsseldorf, Universitätsstrasse 1, D-40225 Düsseldorf, Germany
e-mail: janiak@uni-duesseldorf.de

Contents

1 Introduction

Metal nanoparticles (M-NPs) are of interest for new technologies [1]. The terms "nanoparticles," "nanophase clusters," "nanocrystals," and "(nano-)colloids" are often used with a similar connotation. Here we use the word nanoparticles as a generic term. For applications, it is important to synthesize M-NPs with defined size and small-size distribution in a controlled and reproducible manner [2–6]. A chemical "bottom-up" approach prepares M-NPs by reduction of metal salts or the photolytic, sonolytic, or thermal decomposition of metal–organic precursors [7]. The synthesis conditions such as temperature, solvent, and reducing and stabilizing agent can influence the size, size distribution, and shape of metal nanoparticles [8].

Nanoparticles have a high surface-to-bulk atom ratio and a high surface energy which dominates their properties [9]. A high surface area is, for example, beneficial in (heterogeneous) catalysis [10–16]. Therefore, small M-NPs need to be stabilized; otherwise they will combine to thermodynamically favored larger particles via agglomeration (Fig. 1).

Agglomeration of small particles is based on the principles of Ostwald ripening [17, 18] which is a thermodynamically driven spontaneous process and occurs because larger particles are more energetically favored than smaller ones. Coordinatively, unsaturated surface atoms of a particle are in a higher energy state than well-ordered and fully coordinated atoms in the bulk. The lower the surface area with respect to the bulk volume, the lower the energy state of a particle. A small metal nanoparticle tries to lower its overall energy by detaching atoms from the surface. The atoms then diffuse through the solution and attach to the surface of a larger particle. Thereby, larger particles grow at the expense of smaller particles (Fig. 2).

Small metal nanoparticles can be stabilized by coordination of surface capping ligands, polymers, or surfactants which form a protective electrostatic and/or steric layer to prevent agglomeration (Fig. 1) [19–22]. Metal nanoparticles in ionic liquids (ILs) do not require additional stabilizers. The electrostatic and steric properties of

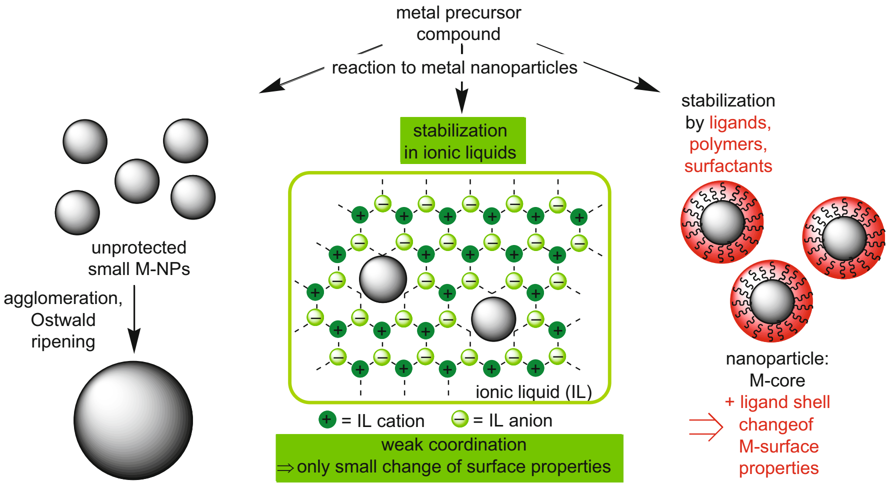

Fig. 1 Metal nanoparticles (M-NP) will agglomerate to larger particles (*left*) unless prevented by electronic and steric stabilization in ionic liquids (*middle*) or through protective stabilizers (*right*)

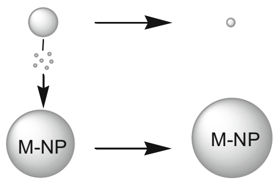

Fig. 2 Schematic presentation of Ostwald ripening

ionic liquids can stabilize M-NPs without capping ligands, polymers, or surfactants (Fig. 1). ILs stabilize metal nanoparticles through their ionic nature [23], high polarity, high dielectric constant, and supramolecular network (cf. Fig. 4) [24–31].

2 Ionic Liquids (ILs)

By definition, ionic liquids are salts with a melting point below 100°C. Typically, ILs are even liquid at room temperature (RT-ILs). For this, they consist of conformationally flexible and weakly coordinating inorganic or organic cations and anions with small lattice enthalpies so that the liquid state is thermodynamically favored [32–36]. Examples of nonfunctionalized IL cations and anions are shown in Fig. 3, and functionalized IL cations in Fig. 5 [12, 43]. ILs have a high charge density, high polarity, and high dielectric constant and form a supramolecular network [28]. Ionic liquids (ILs) have become interesting alternatives to traditional aqueous or organic solvents [44, 45]. Over the last years, they have

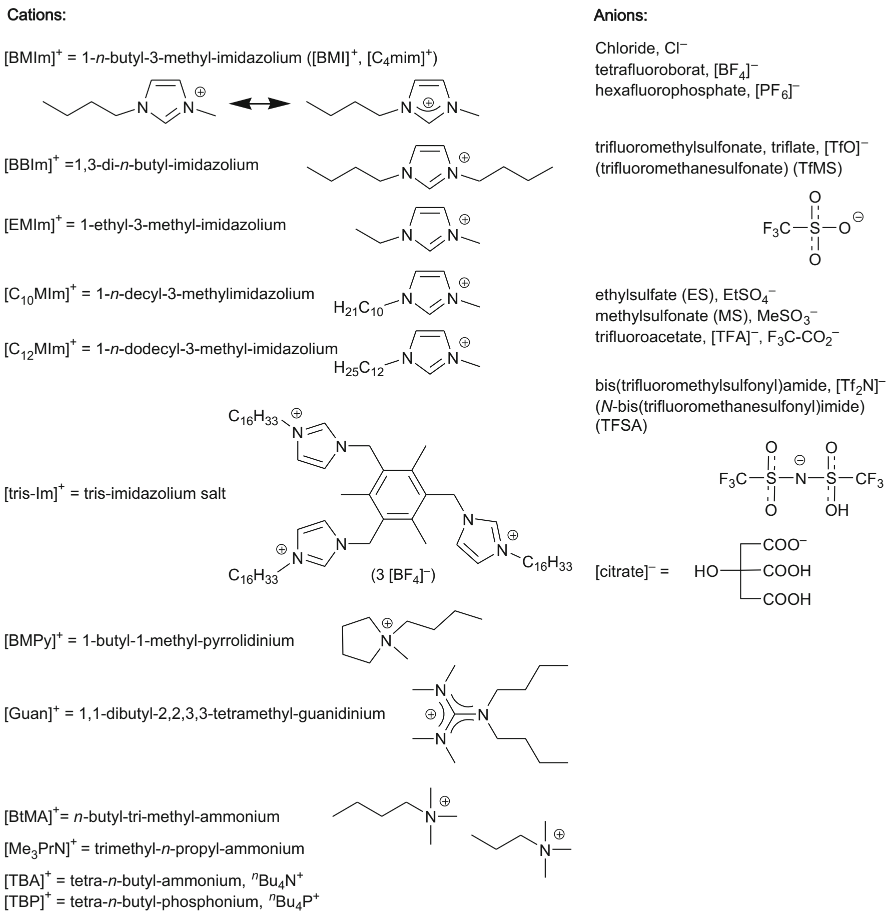

Fig. 3 Cations and anions of nonfunctionalized ILs. For functionalized IL cations see Fig. 5. The abbreviations given in the literature vary

been introduced into solution chemistry and intensively investigated as a new liquid medium [46, 47].

3 Metal Nanoparticles and Ionic Liquids

The preparation of advanced functional materials, including metal nanoparticles, in ILs through ionothermal synthesis, appears highly promising [14, 25, 48–55]. Nanoparticles and ionic liquids go more and more together for materials chemistry [27, 56]. ILs have excellent solvent properties, such as negligible vapor pressure, high thermal stability, high ionic conductivity, a broad liquid-state temperature

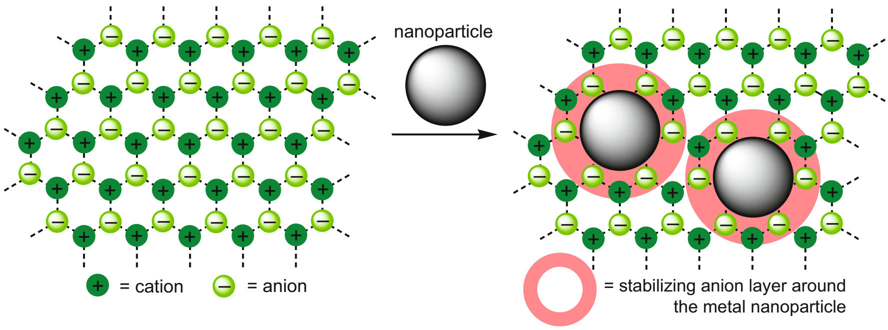

Fig. 4 Schematic network structure in ionic liquids and metal nanoparticles in the IL network. Formation of an anion layer around the M-NPs is suggested for the *electro*static and *steric* (= *electrosteric*) stabilization

range, and the ability to dissolve a variety of materials [57, 58]. The combination of undirected Coulomb forces and directed hydrogen bonds leads to a high attraction of the IL building units. This induces the (high) viscosity, negligible vapor pressure, and three-dimensional network in ILs. Figure 4 suggests how the IL network could provide the needed *electro*static and *steric* (= *electrosteric*) stabilization through the formation of an ion layer around metal nanoparticles [24, 26, 27]. The type of this ion layer, IL-anion or IL-cation, is still a matter of some discussion [27, 37].

ILs provide an electrostatic protection for M-NPs according to DLVO (Derjaguin–Landau–Verwey–Overbeek) theory [59–65] which predicts that the IL-anions should be the primary source of stabilization for the electrophilic metal nanoparticles [59].

Thiol- [38–40], ether- [41], carboxylic acid- [37], amino- [37, 42], hydroxyl- [39, 66, 67], or nitrile- [68–70] functionalized imidazolium cations can stabilize metal NPs even more efficiently through the added functional group (Fig. 5). The OH-functionalized IL [HOEMIm][Tf_2N] gave smaller Pd-NPs with diameter 4.0 ± 0.6 nm compared with Pd-NPs isolated from the nonfunctionalized IL [BMIm][Tf_2N] with diameter 6.2 ± 1.1 nm (cf. Table 1) [67]. The donor atom of the functional group on the cation can attach to the metal nanoparticle like a stabilizing capping ligand possibly together with parallel coordination of the imidazolium plane (Fig. 6) [17, 37, 41, 111–113].

4 Synthesis of Metal Nanoparticles in Ionic Liquids

Metal nanoparticles are obtained in ionic liquids from metal salts by either one of the following ways [114]: (1) chemical reduction [71, 76, 78, 79, 81, 104, 115–118], (2) photochemical reduction [119, 120], or (3) electroreduction/electrodeposition [121–123]. Compounds with zerovalent metal atoms, such as metal carbonyls

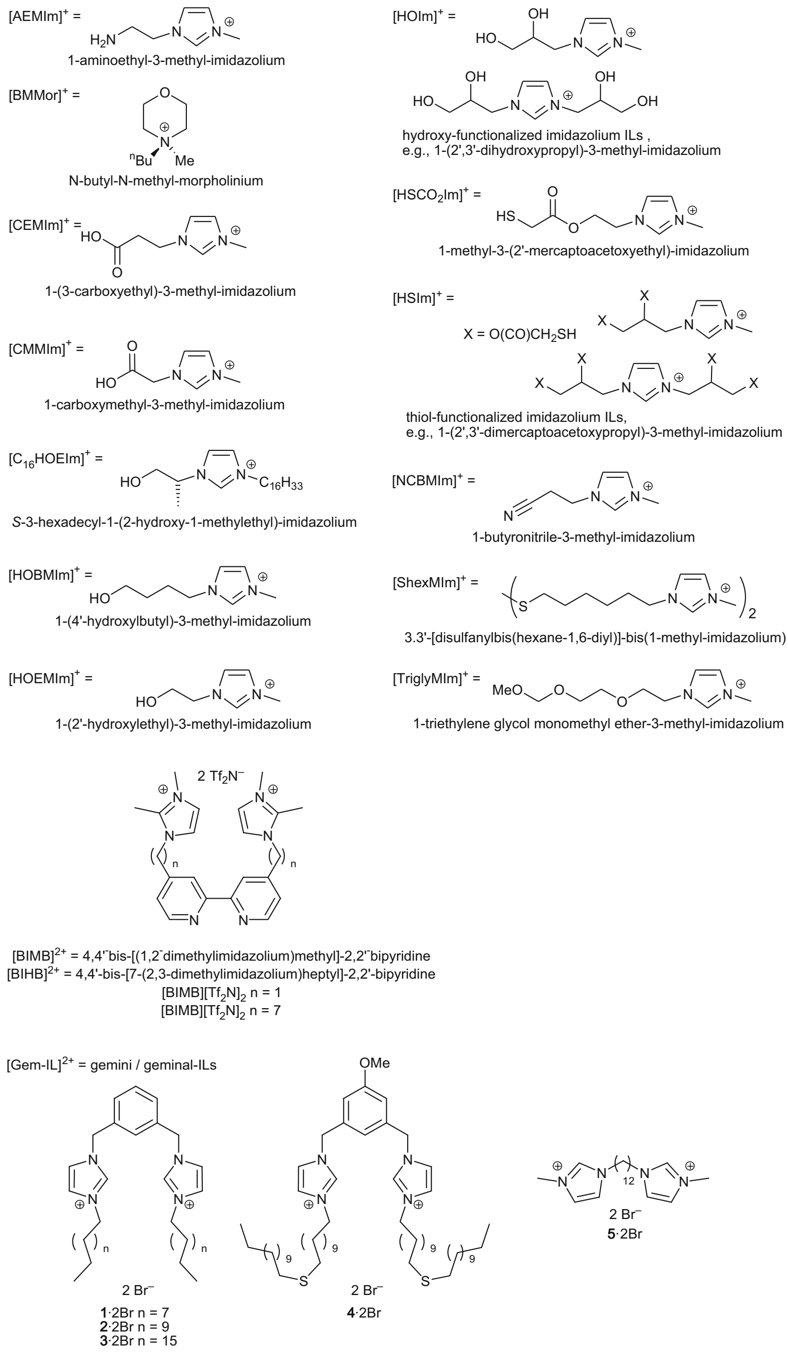

Fig. 5 Examples of functionalized imidazolium cations [37–42]

Table 1 M-NPs prepared by chemical reduction in ILs*

Metal	Metal salt precursor	Reducing agent	Ionic liquid[a]	M-NP average diameter ± standard deviation (nm)	References
Monometallic, group 9 (Rh, Ir)					
Rh	$RhCl_3 \cdot 3H_2O$	H_2, 75°C and 4 bar	[BMIm][PF_6]	2.0–2.5	[71]
	[Rh(COD)-μ-$Cl]_2$[b]	H_2 + laser radiation	[BMIm][PF_6]	7.2 ± 1.3	[72]
	$RhCl_3$	$NaBH_4$	[BMIm][Tf_2N]/[BIMB][$Tf_2N]_2$ or [BIHB][$Tf_2N]_2$	1–3	[73]
Ir	[Ir(COD)$Cl]_2$[b]	H_2, 75°C, and 4 bar	[BMIm][BF_4], [BMIm][PF_6], [BMIm]TfO^-	2–3	[74, 75]
	[Ir$(COD)_2$]BF_4, [Ir(COD) $Cl]_2$[b]	H_2	[1-alkyl-3-methyl-Im][BF_4]	Irregular 1.9 ± 0.4, 3.6 ± 0.9	[76]
Group 10 (Pd,Pt)					
Pd	H_2PdCl_4	$NaBH_4$	[$HSCO_2$Im][Cl]	Nanowires	[40]
	H_2PdCl_4	$NaBH_4$	[Guan][Br]/Vulcan-72 carbon	~2.8	[77]
	$PdCl_2$	H_2 + laser radiation	[BMIm][PF_6]	4.2 ± 0.8	[72]
	$Pd(acac)_2$	H_2	[BMIm][PF_6]	10 ± 0.2	[78]
	$Pd(acac)_2$	Imidazolium ILs, thermal, see text	[BMIm][PF_6], [HOBMIm][Tf_2N]	5, 10, catalysts for selected acetylene hydrogenation	[78]
	$Pd(OAc)_2$ or $PdCl_2$	Imidazolium ILs, ultrasound, see text	[BBIm][Br], [BBIm][BF_4]	20, catalyst for Heck reactions	[79, 80]
	$Pd(OAc)_2$	[BMIm][Tf_2N], thermal	[BMIm][Tf_2N]/PPh_3	~1, catalyst for Heck reactions	[80, 81]
	$Pd(OAc)_2$	Imidazolium ILs, thermal, see text	[HOEMIm][TfO]	2.4 ± 0.5	[67]
			[HOEMIm][TFA]	2.3 ± 0.4	
			[HOEMIm][BF_4]	3.3 ± 0.6	
			[HOEMIm][PF_6]	3.1 ± 0.7	
			[HOEMIm][Tf_2N]	4.0 ± 0.6	
			[BMIm][Tf_2N]	6.2 ± 1.1	

(continued)

Table 1 (continued)

Metal	Metal salt precursor	Reducing agent	Ionic liquid[a]	M-NP average diameter ± standard deviation (nm)	References
	$Pd(OAc)_2$		[TBA][Br]/[TBA][OAc]	3.3 ± 1.2, catalyst for Heck arylations	[80, 82, 83]
	$Pd(OAc)_2$		[BtMA][Tf_2N]	Catalyst for Heck cross-coupling	[80, 84]
	$Pd(OAc)_2$	Imidazolium IL, thermal, see text	[NCBMIm][Tf_2N]	7.3 ± 2.2	[85]
	$Pd_2(dba)_3$[c]	H_2, 3 atm	[tris-Im][BF_4]$_3$, see Fig. 3	Catalyst for Suzuki cross-coupling	[80, 86]
	Bis(benzothiazolylidene carbene)PdI_2		[TBA][Br]/[TBA][OAc]	Catalyst for Heck arylations	[82]
Pt	$Na_2Pt(OH)_6$	$NaBH_4$	[HSIm][A] or [HOIm][A], A = Cl^- or HS-$(CH_2)_3$-SO_3^-	3.2 ± 1.1, 2.2 ± 0.2, 2.0 ± 0.1	[39]
	H_2PtCl_6	$NaBH_4$	[CMMIm][Cl], [AEMIm][Br]	2.5	[37]
	PtO_2	H_2	[BMIm][BF_4], [BMIm][PF_6]	2–3	[87]
	$Pt_2(dba)_3$[c]	H_2, 75°C, 4 atm	[BMIm][PF_6]	2.0–2.5	[88]
	(MeCp)$PtMe_3$	Imidazolium ILs, MWI, hv, thermal, see text	[BMIm][BF_4], [BtMA][Tf_2N]	1.5 ± 0.5, see text; catalyst for hydrosilylation	[89]
Group 11 (Cu, Ag, Au)					
Cu	$Cu(OAc)_2 \cdot H_2O$	$H_2NNH_2 \cdot H_2O$ (hydrazine hydrate)	[BMIm][BF_4]	Spherical; PVP, 80–130; PVA, 260	[90]
			[BMIm][PF_6] Each w. 1% PVP or PVA as stabilizer[d]	Cubic, PVP: 160 ± 14; catalyst in click reaction	
	Cu(I)-amidinate, $\{[Me(C(N^iPr)_2]Cu\}_2$	Imidazolium IL, thermal, see text	[BMIm][BF_4]	11 ± 6	[189]

Ag	$AgBF_4$	H_2, 85°C, 4 atm	[BMIm][BF_4]	2.8 ± 0.8	[91]
			[BMIm][PF_6]	4.4 ± 1.3	
		BIm as scavenger, see text	[BMIm][TfO]	8.7 ± 3.4	
			[BtMA][Tf_2N]	26.1 ± 6.4	
	$AgBF_4$	H_2	[BMIm][BF_4]	~9 (DLS)	[92]
			[BMpy][TfO] with TX-100/cyclohexane as reverse micellar system	~11 (DLS), both ~3 from TEM	
	$AgBF_4$	[BMIm][BH_4], 1-MeIm as scavenger	[BMIm][Tf_2N] in microfluidic reactor	3.73 ± 0.77	[93]
	Ag_2CO_3	Me_2NCHO (DMF)	[Me_2NH_2][Me_2NCO_2] with small amounts of DMF	2–14	[94]
	$AgNO_3$	Tween 85	[BMIm][PF_6]	3–10	[95]
Au	$HAuCl_4$	Na_3citrate/$NaBH_4$, Na_3citrate, ascorbic acid	[EMIm][$EtSO_4$]	9.4 3.9 nanorods	[96]
	$HAuCl_4$	Ascorbic acid	[BMIm] [$C_{12}H_{25}OSO_3$] (lauryl sulfate)	20–50	[97]
	$HAuCl_4$	Na_3citrate	[CMMIm][Cl], [AEMIm][Br]	23–98	[37]
	$HAuCl_4 \cdot 3H_2O$	$H_2NNH_2 \cdot H_2O$ (hydrazine monohydrate)	[TriglyMIm][$MeSO_3$]	~7.5	[41]
	$HAuCl_4$	$NaBH_4$	[ShexMIm][Cl]	5.0	[38]
	$HAuCl_4$	$NaBH_4$	[HSIm][A] or [HOIm][A], A = Cl^- or HS-$(CH_2)_3$-SO_3^-	3.5 ± 0.7, 3.1 ± 0.5, 2.0 ± 0.1	[39]
	$HAuCl_4$	$NaBH_4$	[CMMIm][Cl], [AEMIm][Br]	3.5	[37]
	[C_{16}HOEIm]$AuCl_4$ from [C_{16}HOEIm]Br and $HAuCl_4$	$NaBH_4$	$CHCl_3$/H_2O, [C_{16}HOEIm][Br]	6.0 ± 1.4	[98]

(continued)

Table 1 (continued)

Metal	Metal salt precursor	Reducing agent	Ionic liquid[a]	M-NP average diameter ± standard deviation (nm)	References
	$HAuCl_4$	$NaBH_4$	$[Gem\text{-}IL][Br]_2$ **1**·2Br to **4**·2Br, see Fig. 5	**3**: 8.8 ± 2.2 **4**: 5.3 ± 2.4	[99]
	$HAuCl_4$	$NaBH_4$	$[BMIm][BF_4]$ in microfluidic reactor	4.38 ± 0.53	[100]
	$HAuCl_4$	$NaBH_4$	$[BMIm][PF_6]$	4.8 ± 0.7 (5.3 ± 0.8 after 2 weeks)	[101]
	$HAuCl_4$	$NaBH_4$	$[BMIm][PF_6]/[AEMIm][PF_6]$	4.3 ± 0.8	[101]
	$HAuCl_4$	$NaBH_4$	$[C_{12}MIm][Br]$	8.2 ± 3.5, stable for at least 8 months	[102]
	$HAuCl_4$	$NaBH_4$	$[Gem\text{-}IL][Br]_2$ **5**·2Br, see Fig. 5	10.1 ± 4.2	[102]
	$HAuCl_4$	$[BMIm][BH_4]$, 1-MeIm as scavenger	$[BMIm][Tf_2N]$ in microfluidic reactor	4.28 ± 0.84	[93]
	$HAuCl_4{\cdot}3H_2O$	$NaBH_4$, cellulose	[BMIm][Cl]	9.7 ± 2.7	[103]
	$HAuCl_4$	Cellulose, see text	[BMIm][Cl]	300–800	[104]
	$HAuCl_4{\cdot}3H_2O$	Glycerol	[EMIm][TfO], $[EMIm][MeSO_3]$, $[EMIm][EtSO_4]$	5–7, low temperature 5–7, aggregate at higher temperature 15–20, polydisperse	[105]
	$HAuBr_4$	Me_2NCHO (DMF)	$[Me_2NH_2][Me_2NCO_2]$ with small amounts of DMF	2–4	[94]
	Au(CO)Cl	Imidazolium ILs, thermal, MWI, hν, see text	$[BMIm][BF_4]$	1.8 ± 0.4, 4.1 ± 0.7	[106]
	$KAuCl_4$	$[BMIm][BF_4]$ thermal, see text	$[BMIm][BF_4]$	1.1 ± 0.2	[106]

	$HAuCl_4 \cdot 4H_2O$	$[Me_3NC_2H_4OH]$ $[Zn_nCl2_{n+1}]$, thermal	$[Me_3NC_2H_4OH]$ $[Zn_nCl_{2n+1}]$	135°C: 35 ± 12, 140°C: 30 ± 4, 145°C: 24 ± 3	[107]
	$HAuCl_4 \cdot 3H_2O$,	$[BMIm][BF_4]$, ultrasound, see text	$[BMIm][BF_4]$/MWCNT[e]	10.3 ± 1.5	[108]
	$KAuCl_4$	$SnCl_2$	$[BMIm][BF_4]$	2.6–200	[109]
	$AuCl_3 \cdot 3H_2O$	[TBP][citrate]	[TBP][citrate]	15–20	[110]
Group 12 (Zn)					
Zn	Zn(II)-amidinate, $[Me(C(N^iPr)_2]_2Zn$	Imidazolium IL, thermal, see text	$[BMIm][BF_4]$	3 ± 6	[189]
Bimetallic					
Pd-Au 3:1	K_2PdCl_4, $HAuCl_4$	$NaBH_4$	$[BMIm][PF_6]$	5.3 ± 3.0	[101]
			$[BMIm][PF_6]/[AEMIm][PF_6]$	3.6 ± 0.7	[101]
β-CuZn or γ-Cu_3Zn	Cu(I)- and Zn(II)-amidinate, $\{[Me(C(N^iPr)_2]Cu\}_2$, $[Me(C(N^iPr)_2]_2Zn$	Imidazolium IL, thermal, see text	$[BMIm][BF_4]$	β-CuZn: 51 ± 29, pre-catalyst for MeOH formation from syngas, γ-Cu_3Zn: 48 ± 12	[189]

[a]For nonfunctionalized ILs, see Fig. 3; for functionalized ILs, see Fig. 5

[b]*COD* 1,5-cyclooctadiene, *COT* 1,3,5-cyclooctatriene

[c]*dba* bis-dibenzylidene acetone

[d]*PVP* polyvinyl pyrrolidone, *PVA* polyvinyl alcohol

[e]*MWCNT* multiwalled carbon nanotube

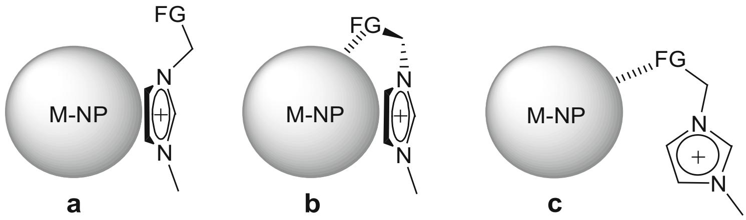

Fig. 6 Possible coordination modes of imidazolium cations with functional groups (FG) to metal nanoparticles [111]

$M_x(CO)_y$ [24, 117, 124, 125] or [Ru(COD)(COT)] (see Sect. 4.6) [91, 126], give metal nanoparticles by thermal, photolytic, or chemical decomposition. Extra stabilizing molecules or organic solvents are not needed in ILs but are added in some cases [19, 24, 27, 65, 127].

4.1 Chemical Reduction

Table 1 compiles metal nanoparticles which have been obtained from the reduction of metal salts and complexes in ionic liquids. Frequent reducing agents are H_2 gas, sodium citrate, ascorbic acid, and imidazolium cations of ILs, $NaBH_4$, or $SnCl_2$.

The synthesis of M-NPs by reduction is carried out in batch reactions using glass flasks, but also microfluidic reactors have been reported for the fabrication of metal nanoparticles of cobalt, copper, platinum, palladium, gold, silver, and core–shell particles [93].

Noble metal nanoparticles, such as Pd- or Ir-NPs, can be synthesized in the presence of imidazolium ILs from metal salts without an added reducing agent [78, 81, 85, 128]. Pd-*N*-heterocyclic carbene complexes may form as intermediates preceding the formation of Pd-NPs (Fig. 7) [79, 80, 128]. Imidazolium salts are precursors for stable carbenes and mild reducing agents [129].

Thermal reduction/decomposition of $Pd(OAc)_2$ to black Pd-NP dispersion in hydroxyl-functionalized ILs with the 1-(2′-hydroxylethyl)-3-methylimidazolium $[HOEMIm]^+$ cation and nonfunctionalized control IL argued against the alcohol group in the $[HOEMIm]^+$ cation as reductant according to unchanged ^1H NMR spectra [67]. The influence of anions on the decomposition rate of $Pd(OAc)_2$ was given in the order $[Tf_2N]^-$, $[PF_6]^- > [BF_4]^- > [OTf]^- > [TFA]^-$.

Decomposition of the organometallic Pt(IV) precursor $(MeCp)PtMe_3$ in the ILs $[BMIm][BF_4]$ and $[BtMA][Tf_2N]$ also does not require a separate reductant and leads to small, crystalline, and longtime stable Pt-nanoparticle (Pt-NP) dispersions (Fig. 8) [89].

The salt $AgBF_4$ can be reduced with H_2 in n-butyl-methyl-imidazolium ionic liquids with different anions to yield Ag-NPs which increase in size with the size of

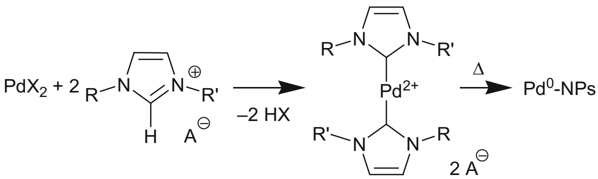

Fig. 7 Pd-carbene formation with imidazolium IL as an intermediate to Pd-NPs [80]

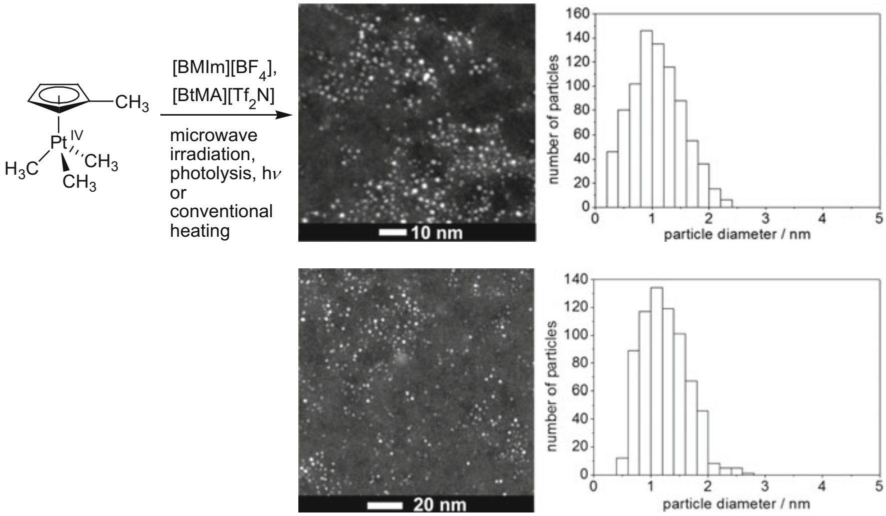

Fig. 8 Decomposition of the air and moisture stable organometallic Pt(IV) precursor (MeCp) $PtMe_3$ in ILs to well-defined, small, crystalline, and longtime (>10 months) stable Pt-nanocrystals without any additional reducing agents. High-angle annular dark-field-scanning transmission electron microscopy (HAADF-STEM) images with particle diameter distributions in histograms, *top row*: freshly prepared sample with NP diameter distribution Ø 1.1 ± 0.5 nm, based on 703 particles; *bottom row*: sample after 331 days, Ø 1.2 ± 0.4 nm, based on 518 particles [89]. Reprinted from [89] with permission from the author; © 2012 The Royal Society of Chemistry

the ionic liquid anion (Fig. 9). The acidic HBF_4 side product needs to be scavenged with a base in order not to perturb the ionic liquid matrix. N-Butylimidazole (BIm) was the base of choice because it gave a $[BHIm]^+$ cation which closely resembled the $[BMIm]^+$ cation (Fig. 9) [115].

Gold nanoparticles are among the best-studied particles in nano- and materials science due to their electronic, optical, thermal, and catalytic properties associated with possible applications in the fields of physics, chemistry, biology, medicine, and materials science [130]. Au-NPs can be reduced from gold salts, e.g., $KAuCl_4$ or auric acid, $HAuCl_4$, by citrate which in addition acts as a coordinating ligand (Turkevich route) [131]. This reduction could also be carried out in the IL 1-ethyl-3-methylimidazolium ethyl sulfate [EMIm][$EtSO_4$] and the Au-NP shape adjusted

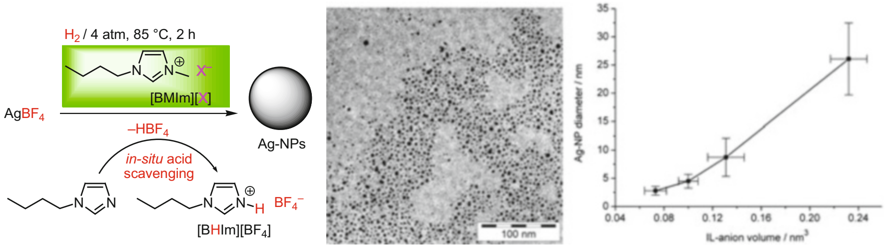

Fig. 9 Formation of Ag-NPs by hydrogen reduction of $AgBF_4$ with an imidazole scavenging process in [BMIm][X]. The TEM image shows the Ag-NPs in [BMIm][BF_4] (Ø 2.8 ± 0.8 nm). The Ag particle size increases with the size of the X^- anion from BF_4^- < PF_6^- < TfO^- < Tf_2N^- [115]. TEM reprinted from [115] with permission from the author; © 2008 American Chemical Society

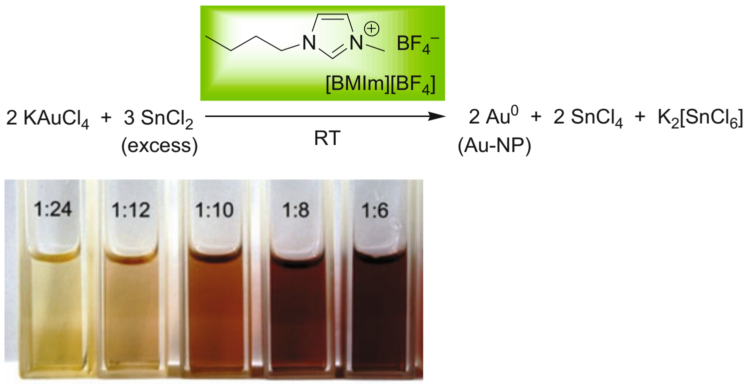

Fig. 10 Selected colors with given molar Au: Sn ratios during the step-by-step Au-NP growth process. The color change represents the transition of Au-NPs from nonmetallic (*white*/*yellow*) to metallic and crystalline (*red* and *purple*) particles. Because of the weakly coordinating nature of the IL, the gold nanoparticle growth can be stopped and resumed here reproducibly by the controlled dropwise addition of a $KAuCl_4$ solution to a mixture of $SnCl_2$/IL at every different color step, which is size dependent for Au-NPs. Such a stop-and-go nanoparticle growth would not be possible in the presence of strongly coordinating capping ligands [109]. Cuvette picture reprinted from [109] with permission from the author; © 2010 The Royal Society of Chemistry

by addition of a silver salt [96]. Cellulose is a reductant, morphology- and size-directing agent for Au-NPs from $HAuCl_4$ so that gold nano-plates with a thickness from 300 nm at 110°C to 800 nm at 200°C were synthesized [104]. Variation of the molar Au(III):Sn(II) ratio gave Au-NPs in different sizes in a stepwise, stop-and-go nucleation, nanocrystal growth process. The Au-NP growth could be stopped and resumed at different color steps and sizes from 2.6 to 200 nm (Fig. 10) [109].

Gold nanoparticles are obtained from Au(CO)Cl or $KAuCl_4$ in imidazolium ILs without an added reducing agent. The reductive thermal, photolytic, or microwave-assisted decomposition was carried out in the presence of *n*-butyl-imidazole as a scavenger (Fig. 11). The nanoparticles of about 1–2 nm diameter in [BMIm][BF_4]

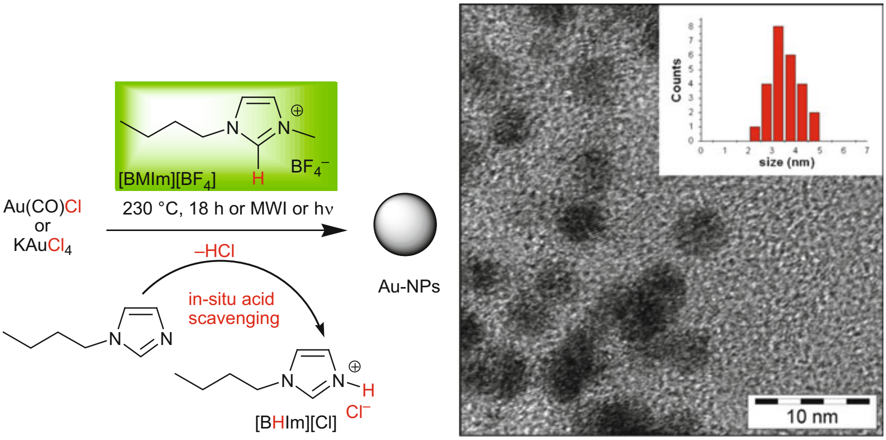

Fig. 11 Formation of Au-NPs (Ø 3.6 ± 0.6 nm from Au(CO)Cl in thermal process) with the imidazole scavenging process in [BMIm][BF_4] (cf. Fig. 9). The TEM picture shows the nanoparticles after 6 weeks of exposure to air [106]. The decomposition of Au(CO)Cl can also proceed by intramolecular reduction under phosgene formation according to 2 Au(CO)Cl → 2 Au + CO + $COCl_2$ [132]. TEM reprinted from [106] with permission from the author; © 2009 Wiley-VCH

increase in size with the ionic liquid anion in [BMIm][TfO] and [BtMA][Tf_2N] [106].

Small Au-NPs of diameter 1.1 ± 0.2 nm which are formed without any capping ligands or surfactants in the IL [BMIm][BF_4] can be selectively reduced or oxidized (quantized charged). A theoretical density functional theory calculation suggests that the positive or negative cluster charging is accompanied by a switching in the orientation of the ionic shell from anion to cation [133].

$NaAuCl_4$ and $KAuCN_2$ were reduced in [BMIm][PF_6] to gold nanoparticles which were catalysts for the cyclopropanation of alkenes with ethyldiazoacetate to yield cyclopropanecarboxylates. In the IL, the stabilized gold catalysts could be separated and recycled [134].

Carboxylic acid- and amino-functionalized ionic liquids [CMMIm][Cl] and [AEMIm][Br] (cf. Fig. 5) stabilized gold and platinum nanoparticles in an aqueous solution. Smaller Au-NPs (3.5 nm) and Pt-NPs (2.5 nm) were prepared with $NaBH_4$ as reducing agent. Larger gold nanospheres (23, 42, and 98 nm) were synthesized with trisodium citrate. Simultaneous interactions between imidazolium ions and its functional groups and the metal atoms were proposed for the M-NP stabilization (cf. Fig. 6). The metal nanoparticles could be assembled on multiwalled carbon nanotubes. The imidazolium ring moiety of the ionic liquids might interact with the nanotube π-surface and the functional group with the M-NPs surface (cf. Fig. 6c) [37].

The microwave-induced decomposition of the transition metal amidinates $\{[Me(C(N^iPr)_2]Cu\}_2$ and $[Me(C(N^iPr)_2]_2Zn$ in [BMIm][BF_4] gives copper and zinc nanoparticles which are stable in the absence of capping ligands (surfactants)

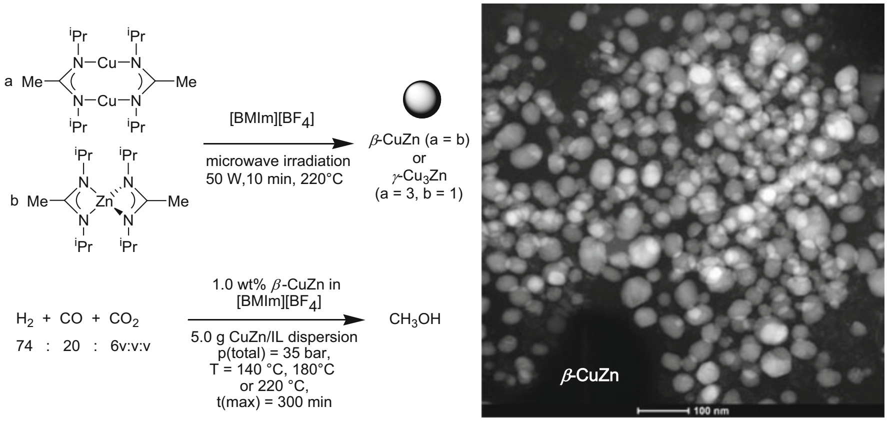

Fig. 12 Microwave-assisted thermal co-decomposition of copper and zinc amidinates to mono-metallic (not shown) and bimetallic Cu/Zn-NPs in IL. The high-angle annular dark-field-scanning TEM (HAADF-STEM) image of a 1.0 wt% β-CuZn dispersion in IL gave a median diameter of 51 ± 29 nm. The β-CuZn/IL dispersion could be employed as precursor for the conversion of syngas to methanol without any catalyst deactivation up to 300 min (5 h) at different temperatures

for more than 6 weeks [189]. Co-decomposition of the two amidinates selectively yields the intermetallic nano-brass phases β-CuZn and γ-Cu_3Zn depending on the chosen molar ratios of the precursors. The bimetallic β-CuZn nanoparticles were precursors to active catalysts for methanol synthesis from syntheses gas H_2/CO/CO_2 with a productivity of 10.7 mol(MeOH)/(kg(Cu)·h) (Fig. 12). STEM investigation of the CuZn/[BMIm][BF_4] dispersion after catalytic methanol formation still showed particles in the 50 nm diameter range as before the catalysis. These particles had a high Cu content by energy-dispersive X-ray spectroscopy (EDX). The regions around the particles were amorphous and contained mostly ZnO according to EDX. Also powder X-ray diffraction of the separated particles revealed that only a fraction of the original β-CuZn phase remained with the rest having turned into crystalline Cu-NPs and amorphous ZnO [189].

From ILs metal nanoparticles can also be deposited onto a support.

Rhodium-NPs (<5 nm) on attapulgite (Rh-Atta) were prepared by reducing immobilized Rh^{3+} on Atta in the IL 1,1,3,3-tetramethylguanidinium lactate. Cyclohexene hydrogenation activity of the Rh-Atta composite was much higher than other catalysts with turnover frequencies reaching 2,700 (mol cyclohexene/mol Rh)/h [135]. Uniform Pd nanoparticles on Vulcan XC-72 carbon were synthesized from H_2PdCl_4 and $NaBH_4$ using G-IL as medium [77].

Hybrids of Au-NP-decorated multiwalled carbon nanotubes (Au-MWCNT) onto poly(ethylene terephthalate) (PET) films were prepared by a sonochemical method from $HAuCl_4$·$3H_2O$ and MWCNT in [BMIm][BF_4] [108]. Au-NPs can also be deposited onto a polytetrafluoroethylene (PTFE, Teflon) surface [106]. Poly(vinylpyrrolidone) (PVP)-stabilized Au-NPs were encapsulated into titania

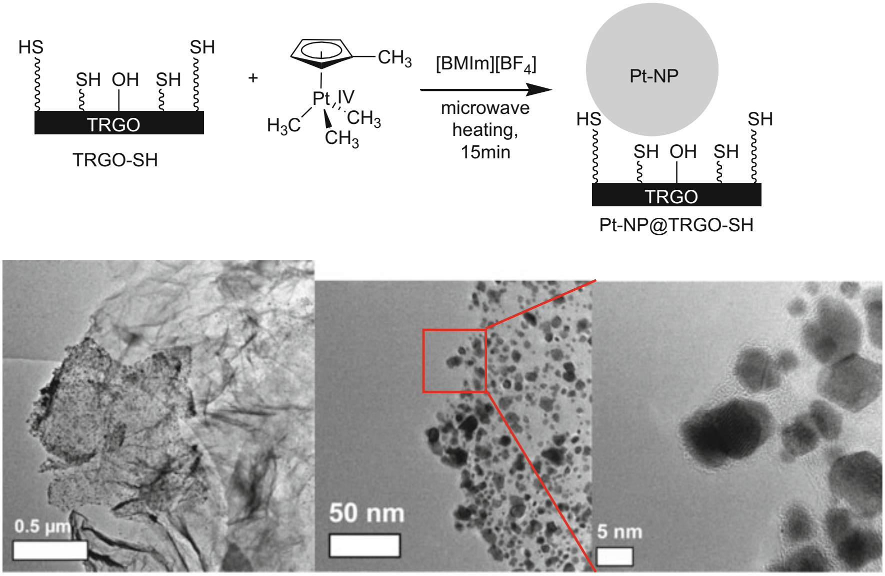

Fig. 13 Schematic presentation of the formation of Pt@TRGO-SH hybrid materials in IL with three magnifications of TEM images. The Pt-NP loading is 3.2 wt% with a median particle diameter of 9 ± 4 nm. Reprinted from [137] with permission from the author; © 2014 Elsevier B.V

xerogels with $[BMIm][PF_6]$ as medium. Then the IL was removed by solvent extraction and the PVP calcinated. The average Au-NP diameter was 8.8 ± 2.5 nm after calcination [136].

Hybrid materials of platinum nanoparticles and thiol-functionalized thermally reduced graphite oxide (TRGO-SH) were synthesized by thermal decomposition of the organometallic precursor $(MeCp)PtMe_3$ in dispersions of TRGO-SH in $[BMIm][BF_4]$ under microwave heating conditions (Fig. 13) [137]. Thiol groups on TRGO assist the deposition of Pt-NPs through a possible dual role of anchor groups and nucleation centers. The IL also helps to exfoliate and separate the graphene sheets in order to increase the surface area and accessibility for deposition of Pt-NPs [137].

4.2 *Photochemical Reduction*

UV photolysis of $(MeCp)PtMe_3$ in $[BMIm][BF_4]$ and $[BtMA][Tf_2N]$ yielded Pt-NPs of 1.1 ± 0.5 nm diameter (1 day old) or 1.2 ± 0.4 nm (aged 331 days) (Fig. 8). Complete decomposition was verified by ^{1}H-NMR spectroscopy through the absence of the characteristic signals from the Pt–Me groups of $(MeCp)PtMe_3$ [89].

Irradiation of $AgClO_4$ with a high-pressure mercury lamp in a mixture of an IL, water, Tween 20 (polyoxyethylene sorbitan monolaurate), and benzoin as photo-activator gave Ag-NPs with average diameters of 8.9 and 4.9 nm in water/[BMIm][BF_4] and water/[OMIm][BF_4] (1-octyl-3-methylimidazolium) microemulsions, respectively [138].

UV irradiation of $HAuCl_4{\cdot}4H_2O$ in a [BMIm][BF_4]/acetone mixture (ratio 10:1) turned the acetone into a free radical which reduced Au(III) to Au nanosheets of about 4 μm length and 60 nm thickness [119]. UV irradiation of $HAuCl_4$ in 1-decyl-3-methyl-imidazolium chloride/water gave differently shaped nanorods with lengths between 100 and 1,000 nm [120]. Photolysis of Au(CO)Cl in [BMIm][BF_4] (cf. Fig. 11) yielded Au-NPs with large diameters of 61 ± 43 nm [106].

4.3 Sonochemical (Ultrasound) Reduction

Ultrasound irradiation of $Pd(OAc)_2$ or $PdCl_2$ in [BBIm][Br] or [BBIm][BF_4] for 1 h yielded nearly spherical Pd-NPs with a diameter of 20 nm. The formation of a Pd–biscarbene intermediate and its subsequent sonolytic conversion to Pd nanoparticles (cf. Fig. 7) was established by NMR/MS and TEM analyses [79].

Au-NP-decorated MWCNT-hybrids were prepared by the ionic liquid-assisted sonication onto PET films. Sonication of a $HAuCl_4{\cdot}3H_2O$, MWCNT, and [BMIm][BF_4] mixture for 60 s gave Au-NPs with narrow size distribution of 10.3 ± 1.5 nm decorated onto the surface of ionic liquid-wrapped MWCNTs [108]. Ultrasound was also used for the synthesis of ionic-liquid-functionalized multiwalled carbon nanotubes decorated with highly dispersed Au nanoparticles from $HAuCl_4{\cdot}3H_2O$ in the presence of 1-(3-aminopropyl)-3-methylimidazolium bromide and dicyclohexylcarbodiimide in DMF solution [139].

4.4 Electro(chemical) Reduction

Ionic liquids are conducting and have a wide electrochemical window of up to 7 V which makes them nearly inert in electrolytic processes. A clean route to prepare metal nanoparticles in ionic liquids is electroreduction with electrons as the only metal-reducing agent (see also Sects. 4.5 and 4.5.2). However, the size of the metal nanoparticles from electroreduction is often above the 100 nm definition limit for nanoparticles.

The technique of pulsed electrodeposition (PED) [140, 141] was used to deposit nanocrystalline Ni [142], Pd [143], Cu [144], Fe [145], Cr [146], and other metals with normal potentials $E^\circ > 0$ V as well as nanoalloys Ni_xFe_{1-x} and Ni_xCu_{1-x} [147] from aqueous electrolytes. Less-noble metals like Al, Mg, and W and their alloys cannot be electrodeposited from aqueous electrolytes but from ionic liquids [140, 141]. Table 2 provides an overview on nanostructured metals which were electrodeposited from ILs.

Table 2 Nano-metals by electrodeposition in ILs

Metal	Metal precursor	Ionic liquid[a]	Size and remarks	References
Monometallic				
Fe	$FeCl_3$, anhydrous	[BMIm][Cl]	40–160 nm by variation of the DC-current density	[148]
Pd	Pd-foil	[BMMor][BF_4]	Nearly 0.5 nm size control with 2.0 ± 0.1, 2.2 ± 0.3, 2.4 ± 0.3, 2.9 ± 0.3, 3.5 ± 0.5, 3.9 ± 0.6, and 4.5 ± 0.9 nm; particle size increased with a decrease in the current density and an increase in temperature and electrolysis duration	[149]
Cu	CuCl	[BMIm][PF_6]	10 nm, at electrode potential of −1.8 V	[150]
Ag	Ag(TfO)	[EMIm][TfO]	Nanowires 3 μm long and 200 nm wide	[151]
Ag@TiO_2	$AgBF_4$	[BMIm][BF_4]	Dendritic network	[152]
Au@PANI	$HAuCl_4 \cdot 3H_2O$	[EMIm][Tos]/ CF_3COOH	500–800 nm Au-NPs distributed in polyaniline (PANI) matrix	[153]
Au@graphene	$HAuCl_4$	[BMIm][PF_6]	10 nm Au-NPs by simultaneous reduction of graphite oxide and $HAuCl_4$ at −2.0 V	[154]
Al	$AlCl_3$, anhydrous	[EMIm][Cl]	Crystallite sizes from 10 to 133 nm with aromatic and aliphatic carboxylic acid additives and by temperature variation	[148]
Bimetallic				
Al_xMn_{1-x}	$MnCl_2$	[BMIm] [Cl]/$AlCl_3$	25	[148]
Al_xIn_{1-x}	$InCl_3$	[BMIm] [Cl]/$AlCl_3$	25	[148]

[a]For nonfunctionalized ILs, see Fig. 3; for functionalized ILs, see Fig. 5

4.5 Gas-Phase Synthesis

Gas-phase synthesis can be divided in gas-phase condensation and flame pyrolysis and is very effective for high purity nanoparticle products. In gas-phase condensation, the metal is vaporized from heated crucibles by electron or laser beam evaporation or sputtering and condensed here onto an ionic liquid. When a precursor compound is decomposed, the process is called chemical vapor condensation or chemical vapor synthesis. In flame pyrolysis, the gaseous or liquid precursors are decomposed by a combustion reaction [155]. The negligible vapor pressure of ILs allows to use them in methods requiring vacuum conditions. For metal nanoparticle synthesis, such methods are magnetron sputtering onto ILs, plasma reduction in ILs, physical vapor deposition onto ILs, and electron beam and γ-irradiation to ILs [34].

4.5.1 Magnetron Sputtering

The sputtering of clusters or atoms onto ILs to give nanoparticles is possible for all elements that can be ejected from a target by Ar^+ and $N_2{}^+$ plasma ion bombardment. Thus, Au, Ag, Pt, and other M-NPs with diameters of less than 10 nm were prepared by magnetron sputtering. The surface tension and viscosity of the IL are important factors for the nanoparticle growth and stabilization [34].

Indium nanoparticles were obtained by sputter deposition of indium into [BMIm][BF_4], [EMIm][BF_4], [(1-allyl)MIm][BF_4], and [(1-allyl)EIm][BF_4]. The In-NP surface was covered by an amorphous In_2O_3 layer as In/In_2O_3 core–shell particles. The size of the In core was tunable from ca. 8 to 20 nm by choice of the IL [156].

Platinum nanoparticles were produced by Pt sputtering onto [Me_3PrN][Tf_2N] with mean particle diameters of 2.3–2.4 nm independent of sputtering time [157].

Gold nanoparticles of 1–4 nm size were prepared by sputter deposition of the metal onto the surface of [BMIm][BF_4] [158] and [BMIm][PF_6] [159]. In the latter, the size of Au nanoparticles was increased from 2.6 to 4.8 nm by heat treatment at 373 K [159]. Au-NPs of 3–5 nm diameter were obtained by sputtering onto several imidazolium ILs [160].

4.5.2 Plasma Deposition Method, Glow-Discharge (Plasma) Electrolysis

A plasma is a gas which is partially ionized, becomes electrically conductive, and has collective behavior. Plasma deposition is also called glow-discharge electrolysis (GDE) [34], plasma electrochemical deposition (PECD) [140, 141, 155], or gas–liquid interfacial discharge plasma (GLIDP) [161]. It is an electrochemical technique in which the discharge is initiated in the gas between a metal electrode and a solution by applying a high voltage. In ionic liquid glow-discharge electrolysis (IL-GDE), the discharge is initiated in the gas between the metal electrode and the ionic liquid solution. The plasma is regarded as an electrode because of the deposition of the materials at the interface of ionic liquid and plasma. In IL-GDE the precursor material is dissolved in the IL and is reduced with free electrons from the plasma [155, 162]. Table 3 lists metal nanoparticles which were obtained by IL-GDE.

Table 3 Nanoparticles by plasma deposition method (glow-discharge plasma electrolysis) in ILs

Metal	Metal precursor	Ionic liquid[a]	Average particle diameter ± standard deviation/nm	References
Pd	$PdCl_2$	[BMIm][BF_4]	32.7	[163]
Cu	$Cu(TfO)_2$	[BMPy][TfO]	~40, deposited on gold surface	[164]
	Cu	[EMIm][Tf_2N]	~11	[165]
	Cu	[BMPy][Tf_2N]	~26	[165]
Ag	$AgNO_3$/Ag(TfO)	[BMIm][TfO]	~8–30	[155, 166]
	Ag(TfO)	[EMIm][TfO]	20	[155, 164]
	$AgBF_4$	[BMIm][BF_4], [BMIm][PF_6]	<100, at glassy carbon electrode	[167]
Au	$HAuCl_4$	[BMIm][BF_4]	~2; as Au-NP-DNA encapsulated SWNTs[b]	[161]
	$HAuCl_4 \cdot 4H_2O$	[BMIm][BF_4]	1.7 ± 0.8, in presence of PVP[c]	[168]
Al	$AlCl_3$	[BMPy][Tf_2N]	~34, 20–64, deposited on gold surface	[164]
Ge	$GeCl_2$ dioxane	[EMIm][Tf_2N]	<50	[169]

[a]For nonfunctionalized ILs, see Fig. 3; for functionalized ILs, see Fig. 5
[b]*SWNTs* single-walled carbon nanotubes
[c]*PVP* polyvinylpyrrolidone

4.5.3 Physical Vapor Deposition Method

Physical vapor deposition uses laser beam evaporation of the metal and condensation onto an ionic liquid under vacuum. It offers an easy and fast method for the preparation of stable metal and metal-oxide particles. The use of nonvolatile ILs avoids the otherwise needed freezing of the solvent as well as additional stabilizers [170].

Evaporization of elemental Cu powder under high vacuum (10^{-6} Torr) onto the surface of [BMIm][PF_6] or [BMIm][Tf_2N] generated Cu nanoparticles with an average diameter of 3 nm. Cu metal was also vaporized into an IL dispersion of ZnO to give Cu-NPs with ~3.5 nm diameter on or near the ZnO surface [170]. Gas-phase deposition gave Au-NPs whose average diameter (∅) depended on the IL: [BMIm][BF_4] ∅ 7 nm, [BMIm][Tf_2N] ∅ 4 nm, [BMPy][Tf_2N] ∅ 20–40 nm, [BMIm][DCA] (DCA = dicyanamide) initial ∅ 10 nm, later 40–80 nm, and [P_{66614}][DCA] (P_{66614} = trishexyltetradecylposphonium) ∅ 50 nm [170].

4.5.4 Electron Beam and γ-Irradiation

Very strong electron beam and γ-irradiation of an IL with a dissolved metal salt yield solvated reducing electrons and/or radicals which generate the metal nanoparticles [34].

Accelerator electron beam and γ-irradiation of $NaAuCl_4 \cdot 2H_2O$ gave Au-NPs at 6 and 20 kGy in [BMIm][Tf_2N]. From accelerator electron beam irradiation, spherical Au nanoparticles were formed with a mean diameter of 7.6 ± 1.5 nm at 6 kGy irradiation and of 26.4 ± 3.7 nm at 20 kGy. The γ-irradiation gave smaller

Au-NPs with 2.9 ± 0.3 nm and 10.7 ± 1.7 nm at 6 kGy and 20 kGy, respectively, in [BMIm][Tf_2N]. It was emphasized that the prepared Au-NPs were stable without the need for a coordinating additive for more than 3 months [171]. A low-energy electron beam irradiation was used to synthesize 122 nm Au-NPs from $NaAuCl_4 \cdot 2H_2O$ in [BMIm][Tf_2N] [172].

4.6 *Metal Nanoparticles from Zerovalent Metal Precursors*

4.6.1 Metal Nanoparticles from Metal Carbonyls, $M_x(CO)_y$

The binary metal carbonyls $Cr(CO)_6$, $Mo(CO)_6$, $W(CO)_6$, $Mn_2(CO)_{10}$, $Re_2(CO)_{10}$, $Fe(CO)_5$, $Fe_2(CO)_9$, $Fe_3(CO)_{12}$, $Ru_3(CO)_{12}$, $Os_3(CO)_{12}$, $Co_2(CO)_8$, $Co_4(CO)_{12}$, $Rh_4(CO)_{12}$, $Rh_6(CO)_{16}$, $Ir_4(CO)_{12}$, and $Ni(CO)_4$ are commercially available from Aldrich, ABCR, or Acros. $Fe(CO)_5$ and $Ni(CO)_4$ are industrially produced on a multiton scale [173]. Most metal carbonyls $M_x(CO)_y$ are easily purified and handled, even if care should be exerted for the possible liberation of poisonous CO. The metal carbonyls contain the metal atoms already in the zerovalent oxidation state, and a reducing agent is not needed for M-NP synthesis. The side product CO is removed through the gas phase. Thus, contamination from by- or decomposition products is greatly reduced. Hence, metal carbonyls were already long used for the preparation of M-NPs but without ILs. Much of the work on Fe- or Co-NPs from $M_x(CO)_y$ dealt with magnetic NPs [174].

Metal nanoparticles were reproducibly obtained by conventional thermal decomposition (180–250°C, 6–12 h), by UV photolysis (1,000 W, 15 min), or by easy, rapid (few minutes), and energy-saving (as low as 10 W) microwave irradiation (MWI) under an argon atmosphere from their metal carbonyl precursors $M_x(CO)_y$ in ILs (Fig. 14, Table 4). The M-NP synthesis in IL from $M_x(CO)_y$ again does not require any additional stabilizers, surfactants, or capping molecules to give long-term stable M-NP/IL dispersions [30, 31].

Ionic liquids have a significant absorption efficiency for microwave energy because of their high ionic charge, high polarity, and high dielectric constant and, thus, are attractive media for microwave reactions [35]. Microwave heating is extremely rapid. The low-frequency energy source of microwaves is remarkably adaptable to many types of chemical reactions [179]. Microwave radiation can interact directly with the reaction components. The reactant mixture absorbs the microwave energy and localized superheating occurs resulting in fast and efficient heating times [180, 181]. The use of microwaves is a rapid way to heat reactants compared with conventional thermal heating. Any presumptions about abnormal "microwave effects" [182–184] have been proven wrong in the meantime [185, 186]. Microwaves are also an "instant on/instant off" energy source which reduces the risk of overheating reactions [179, 180].

Complete $M_x(CO)_y$ decomposition from the short 3–10-min microwave irradiation was verified by Raman or IR spectroscopy through the absence of (metal)

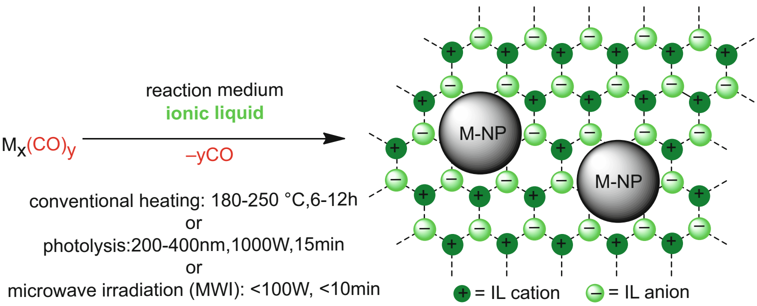

Fig. 14 Schematic presentation for the formation of M-NPs from $M_x(CO)_y$/IL dispersions by conventional thermal heating, photolysis, or microwave-induced heating

carbonyl bands around 2,000 cm^{-1} (Fig. 15) [30, 31, 111, 117]. For W- and Rh-NPs, it was shown that the diameter increases with the molecular volume of the ionic liquid anion (similar to Ag-NPs, cf. Fig. 9) [124].

Examples of TEM pictures of metal nanoparticles obtained by microwave irradiation or UV photolysis from their metal carbonyl precursors $M_x(CO)_y$ in [BMIm][BF_4] are given in Fig. 16 [117].

The synthesis of Co-NPs and Mn-NPs from $Co_2(CO)_8$ and $Mn_2(CO)_{10}$, respectively, in the functionalized IL 1-(3-carboxyethyl)-3-methyl-imidazolium tetrafluoroborate [CEMIm][BF_4] yields smaller and better separated particles (1.6 ± 0.3 nm and 4.3 ± 1.0 nm, respectively) than in the nonfunctionalized IL [BMIm][BF_4] (5.1 ± 0.39 nm and ~29 ± 12 nm, respectively) (see Table 4) under the same conditions which is an indication of a rather strong interaction of the IL-carboxy group with the nanoparticles [111].

4.6.2 Metal Nanoparticles from Zerovalent Metal Precursors Other Than $M_x(CO)_y$

Other organometallic compounds with zerovalent metal atoms are [Ru(COD)(COT)] and [Ni(COD)$_2$] (COD = 1,5-cyclooctadiene, COT = 1,3,5-cyclooctatriene). Hydrogen as a reagent was used to hydrogenate the ligands COD and COT to cyclooctane and thereby dissociate them from the Ru(0) or Ni(0) atom [91, 118, 126, 187]. [Ru(COD)(COT)] and [Ni(COD)$_2$] were dissolved in imidazolium ILs and the mixture heated with 4 bar of hydrogen under different conditions to obtain the metal nanoparticles (Table 5).

Ruthenium nanoparticles from [Ru(COD)(COT)]/H_2 in various 1-alkyl-3-methyl-imidazolium ionic liquids showed a relationship between the Ru-NP diameter and the size of IL nonpolar domains [188]. This suggested that the size of the nanoparticles is governed by the degree of self-organization of the imidazolium ionic liquid in which they are generated: the more structured the ionic liquid, the

Table 4 Examples of M-NPs prepared from metal carbonyls in ILs*

Metal	Metal carbonyl precursor	Ionic liquid[a]	M-NP average diameter ± standard deviation (nm)	Remarks	References
Cr	$Cr(CO)_6$	$[BMIm][BF_4]$, [BMIm][TfO], $[BMIm][Tf_2N]$	≤1.5 ± 0.3, MWI, thermal[b] 4.4 ± 1.0, hν[b]	[c,d,e,f]	[117, 124]
Mo	$Mo(CO)_6$	$[BMIm][BF_4]$, [BMIm][TfO], $[BMIm][Tf_2N]$	~1–2, MWI, hν[b] ≤1.5 ± 0.3, thermal[b]	[c,d,e,f]	[117, 124]
W	$W(CO)_6$	$[BMIm][BF_4]$, [BMIm][TfO], $[BMIm][Tf_2N]$	3.1 ± 0.8, MWI[b] <1, hν[b] ≤1.5 ± 0.3, thermal[b]	[c,d,e,f]; see Fig. 15	[117, 124]
Mn	Mn_2CO_{10}	$[BMIm][BF_4]$	12.4 ± 3, MWI <1, hν 28.6 ± 11.5, MWI	[c,d,e]	[111, 117]
		$[CEMIm][BF_4]$	4.3 ± 1.0, MWI	See text	[111]
Re	Re_2CO_{10}	$[BMIm][BF_4]$	2.4 ± 0.9, MWI <1, hν	[c,d,e]; see Fig. 16	[117]
Fe	$Fe_2(CO)_9$	$[BMIm][BF_4]$	8.6 ± 3.2, MWI[b] 7.0 ± 3.1, hν[b] 5.2 ± 1.6, thermal[b]	[c,d,e,f]	[24, 117]
Ru	$Ru_3(CO)_{12}$	$[BMIm][BF_4]$	1.6 ± 0.3, MWI[b] 2.0 ± 0.5, hν[b] 1.6 ± 0.4, thermal[b]	[c,d,e,f]; see Fig. 16, hydrogenation catalyst, Fig. 18	[24, 117]
		$[BMIm][BF_4]$	2.2 ± 0.4, MWI	Ru-NPs deposited on TRGO, see text, Fig. 19	[175]
Os	$Os_3(CO)_{12}$	$[BMIm][BF_4]$	0.7 ± 0.2, MWI[b] 2.0 ± 1.0, hν[b] 2.5 ± 0.4, thermal[b]	[c,d,e,f]	[24, 117]
Co	$Co_2(CO)_8$	$[BMIm][BF_4]$, [BMIm][TfO], $[BMIm][Tf_2N]$	5.1 ± 0.9, MWI[b] 8.1 ± 2.5, hν[b] 14 ± 8, thermal[b]	[c,d,e,f]	[24, 117]
		$[CEMIm][BF_4]$	1.6 ± 0.3, MWI	See text	[111]

	$Co_2(CO)_8$	$[C_xMIm][Tf_2N]$	7.7, thermal at 150°C	Fischer–Tropsch catalyst giving olefins, oxygenates, and paraffins (C_7–C_{30}), reusable at least three times	[176]
	$Co_2(CO)_8$	$[C_{10}MIm][Tf_2N]$	53 ± 22, thermal at 150°C	Co-NPs with cubic shape together with Co-NPs of irregular shape	[177]
Rh	$Rh_6(CO)_{16}$	$[BMIm][BF_4]$, [BMIm][TfO], $[BMIm][Tf_2N]$	1.7 ± 0.3, MWI[b] 1.9 ± 0.3, hv[b] 3.5 ± 0.8, thermal[b]	[c,d,e,f]; hydrogenation catalyst	[24, 117]
		$[BMIm][BF_4]$	2.8 ± 0.5	Rh-NPs deposited on TRGO, see text, Fig. 19	[175]
		$[BMIm][BF_4]$	2.1 ± 0.5	Rh-NPs deposited on Teflon-coated stirring bar, see text, Fig. 20	[178]
Ir	$Ir_4(CO)_{12}$	$[BMIm][BF_4]$, [BMIm][TfO], $[BMIm][Tf_2N]$	0.8 ± 0.2, MWI[b] 1.4 ± 0.3, hv[b] 1.1 ± 0.2, thermal[b]	[c,d,e,f]; see Fig. 15, hydrogenation catalyst	[24, 117]

*Table reprinted from Z. Naturforsch., 2013, 68b, 1059–1089. Copyright Verlag der Zeitschrift für Naturforschung, Tübingen 2013

[a]For nonfunctionalized ILs, see Fig. 3; for functionalized ILs, see Fig. 5

[b]In $[BMIm][BF_4]$

[c]Median diameters and standard deviations are from TEM measurements

[d]Microwave decomposition of metal carbonyls with 10 W for 3–10 min

[e]Photolytic decomposition of metal carbonyls with a 1000 W Hg lamp (200–450 nm wavelength) for 15 min

[f]Thermal decomposition of metal carbonyls from 6 to 12 h with 180–230°C depending on the metal carbonyl

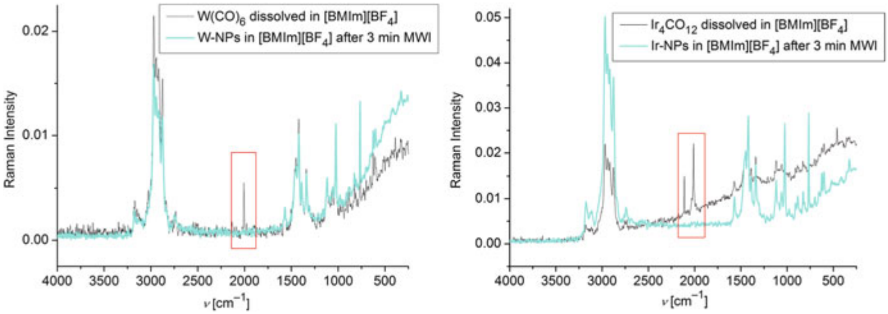

Fig. 15 Raman–Fourier-transform spectra of $W(CO)_6$ and $Ir_4(CO)_{12}$ in [BMIm][BF_4] before and after 3 min 10 W microwave irradiation (MWI). *Red boxes* highlight the indicative metal carbonyl bands [117]. Adapted from [117] with permission from the author; © 2010 Wiley-VCH

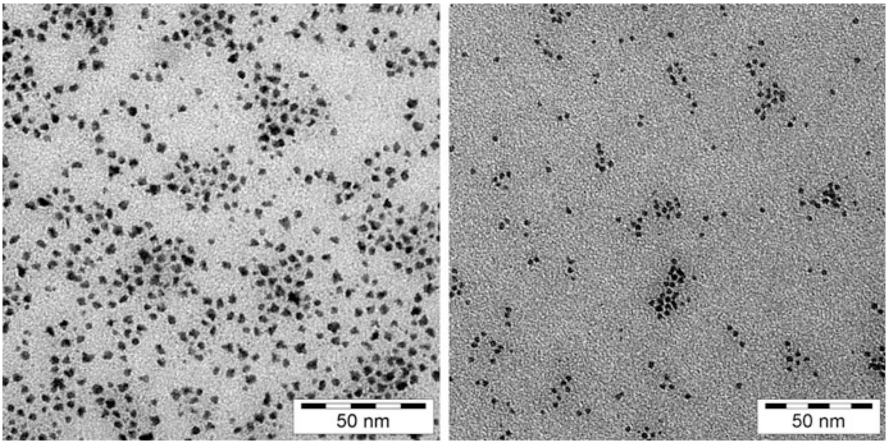

Fig. 16 TEM photographs. *Left*: Re-NPs from $Re_2(CO)_{10}$ by MWI in [BMIm][BF_4], ∅ 2.4 ± 0.9 nm. *Right*: Ru-NPs from $Ru_3(CO)_{12}$ by photolysis in [BMIm][BF_4], ∅ 2.0 ± 0.5 nm (cf. Table 4) [117]. Reprinted from [117] with permission from the author; © 2010 Wiley-VCH

smaller the size [91]. The stabilization of Ru-NPs in imidazolium ILs is further related to the presence of surface hydrides and their confinement in nonpolar domains due to the continuous 3-D network of ionic channels [191].

Very small (ca. 1.2 nm) and stable Ru-NPs were obtained from [Ru(COD)(COT)]/H_2 in the imidazolium ILs [C_xMIm][Tf_2N] ($C_x = C_nH_{2n+1}$ where $n = 2$, 4, 6, 8, 10) in the presence of amine ligands (1-octylamine, 1-hexadecylamine) which act as coordinating ligands [192].

$Ni(COD)_2$ also decomposes thermally in 1-alkyl-3-methylimidazolium bis(trifluoromethylsulfonyl)amide ionic liquids [118] or in [BMIm][BF_4] under microwave heating to Ni nanoparticles [193]. Thermal co-decomposition of [$Ni(COD)_2$] and GaCp* in [BMIm][BF_4] in 1:1 or 1:3 molar ratio gave the stable nanoalloys NiGa and Ni_3Ga, respectively (Fig. 17) [193].

Table 5 Examples of M-NPs prepared in ILs from zerovalent metal precursors other than $M_x(CO)_y$

Metal	Metal precursor[b]	IL[a]	M-NP diameter ± standard deviation (nm)		References
Ru	[Ru(COD)(COT)]	[BMIm][Tf_2N]	0.9–2.4		[91]
		[BMIm][Tf_2N] w. H_2O or 1-octylamine (OA)	H_2O: ~2 nm NPs grouped in circular aggregates of 20–30 nm; OA with OA/Ru > 0.1: 1.1 ± 0.3		[126]
			25°C, stirring	0°C, no stirring	[188]
		[EMIm][Tf_2N]	2.4 ± 0.3	2.3 ± 0.6	
		[BMIm][Tf_2N]	2.3 ± 0.3	1.1 ± 0.2	
		[C_6MIm][Tf_2N]		1.9 ± 0.6	
		[C_8MIm][Tf_2N]	3.6 ± 1.6	2.3 ± 0.8	
		[C_{10}MIm][Tf_2N]	Sponge-like superstruct., >100–150		
		[BBIm][Tf_2N]	2.3 ± 0.6	2.0 ± 0.6	
		[BMMIm][Tf_2N][c]	2.4 ± 0.3	1.8 ± 0.5	
		[BMIm][BF_4], [BMIm][PF_6], [BMIm][TfO]	2.6 ± 0.4		[187]
Ni	[$Ni(COD)_2$]	[C_xMIm][Tf_2N]	4.9 ± 0.9 to 5.9 ± 1.4		[118]
		[BMIm][BF_4]	10 ± 4		[193]
Bimetallic					
NiGa or Ni_3Ga	[$Ni(COD)_2$], GaCp*[d]	[BMIm][BF_4]	NiGa: 14 ± 9, semihydrogenation catalyst; see Fig. 17; Ni_3Ga: 17 ± 8		[193]

[a]For nonfunctionalized ILs, see Fig. 3; for functionalized ILs, see Fig. 5
[b]*COD* 1,5-cyclooctadiene, *COT* 1,3,5-cyclooctatriene
[c][*BMMIm*]$^+$ 1-butyl-2,3 dimethyl-imidazolium
[d]*Cp** pentamethylcyclopentadienyl

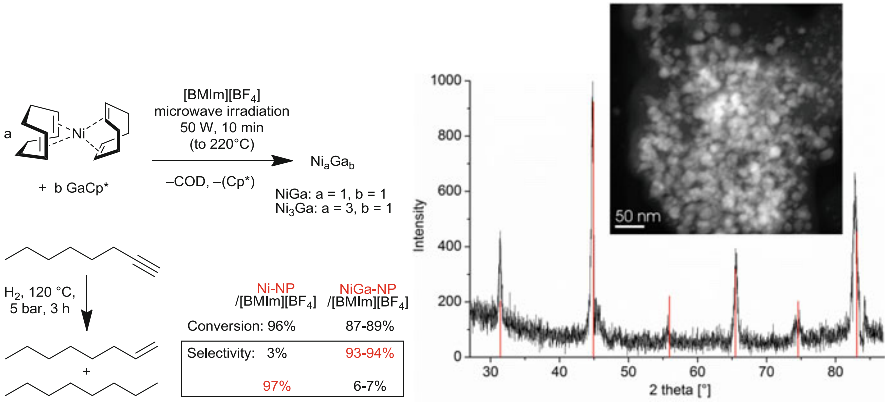

Fig. 17 Microwave-assisted thermal co-decomposition of [Ni(COD)$_2$] and GaCp* to bimetallic Ni/Ga-NPs in IL. The high-angle annular dark-field-scanning TEM (HAADF-STEM) image of a 1.0 wt% NiGa dispersion in IL gives diameters between 7 and 29 nm (average 14 $\pm$ 9 nm). PXRD provides evidence for NiGa as the single crystalline component with reference data in *red* taken from ICSD No: 103854 (NiGa). The slightly broadened reflections suggest crystallite domain sizes of 21 $\pm$ 10 nm as calculated with the Scherrer equation [190]. The NiGa/IL dispersion could be employed for the catalytic semihydrogenation of 1-octyne or diphenylacetylene (tolan, not depicted) to 1-octene or diphenylethylene in about 90% yield and with up to 94 or 87% selectivity, while Ni-NPs under the same conditions yield the alkanes in 97 or 78% selectivity, respectively [193]

4.6.3 Catalytic Applications of Metal Nanoparticles Derived from $M_x(CO)_y$

Nonfunctional ionic liquids contain only weakly coordinating cations and anions (see Fig. 3) which bind less strongly to the M-NP surface than coordinating capping or protective ligands. Hence, metal nanoparticles in ILs should be effective catalysts, and a number of catalytic reactions have successfully been carried out in ILs [12, 194]. Nonvolatile ILs fit into the context of “green catalysis” [195] which requires that catalysts be designed for easy separation from the reaction products and multi-time efficient reuse [35, 196, 197]. The miscibility of ILs with organic substrates can be designed to allow for phase separation and decantation [197] or removal of volatile products by distillation in vacuum. At the same time, the IL is able to retain the M-NPs for catalyst reuse and recycling. It was already demonstrated that M-NP/IL systems were quite easily recyclable and reusable for several times without significant catalytic deactivation [24]. In hydrogenation reactions with Rh- or Ru-NP/IL systems, the catalytic activity did not decrease upon repeated reuse [117, 124]. The catalytic properties (activity and selectivity) put dispersed M-NPs closer to heterogeneous (multisite, surface-like) than to homogeneous (single-site) catalysts [198, 199].

The hydrogenation of internal alkynes with Pd-NPs at 25°C under 1 bar of hydrogen yields Z-alkenes with up to 98% selectivity. At higher hydrogen pressure

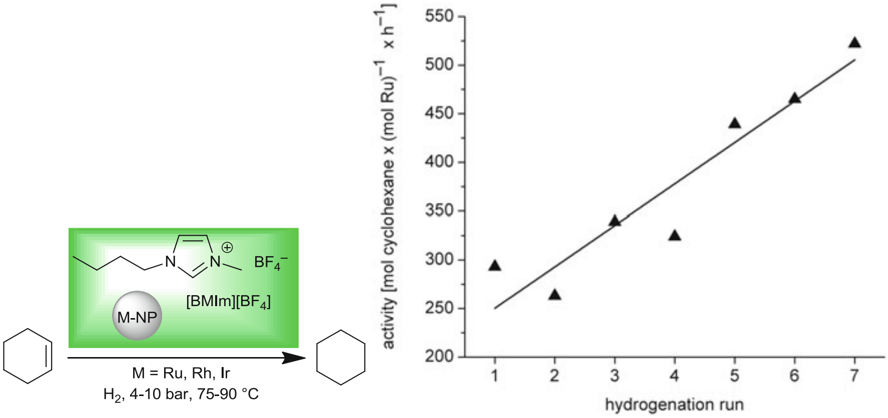

Fig. 18 Hydrogenation of cyclohexene to cyclohexane with Ru-, Rh-, or Ir-NP/IL. Activity even increases over seven runs with the same Ru-NP/[BMIm][BF_4] catalyst at 90°C, 10 bar H_2 pressure. Conversion was intentionally stopped at 95% as thereafter the decrease in cyclohexene concentration lowered the reaction rate [117]. Rh- and Ir-NP/[BMIm][BF_4] gave activities of 1,900mol cyclohexane × (mol Ir)$^{-1}$ × h^{-1} and 380 mol cyclohexane × (mol Rh)$^{-1}$ × h^{-1} for quantitative conversion at 4 bar H_2 pressure and 75°C [124]

(4 bar), alkanes were exclusively obtained without detection of any alkenes. TOF values reached 1,282 h^{-1} with good recyclability of the system and no loss of activity for at least four runs [85].

Ru-, Rh-, and Ir-NP/[BMIm][BF_4] dispersions were active catalysts in the organic-solvent-free hydrogenation of cyclohexene or benzene to cyclohexane (Fig. 18) [30, 31, 117]. Also, a remarkable partial hydrogenation of benzene to cyclohexene with Ru-NP/[BMIm][PF_6] has been reported [187].

Ruthenium or rhodium nanoparticles could be supported on thermally reduced graphite oxide (TRGO, "graphene") with small and uniform particle sizes (Ru 2.2 ± 0.4 nm and Rh 2.8 ± 0.5 nm) from $Ru_3(CO)_{12}$ and $Rh_6(CO)_{16}$, respectively, through microwave irradiation of a $M_x(CO)_y$/TRGO/[BMIm][BF_4] mixture (Fig. 19). The hybrid materials Rh-NP@TRGO and Ru-NP@TRGO were directly catalytically active in hydrogenation reactions. The recyclable M-NP@TRGO nanocomposites gave a complete conversion of cyclohexene or benzene to cyclohexane under organic-solvent-free conditions (50–75°C, 4 bar H_2) with reproducible and steady activities of 1,570 mol cyclohexene × (mol Ru)$^{-1}$ × h^{-1} and 310 mol benzene × (mol Rh)$^{-1}$ × h^{-1} (Fig. 19) [175].

Rhodium nanoparticles could be deposited onto a standard Teflon-coated magnetic stirring bar which is present during microwave decomposition of $Rh_6(CO)_{16}$ in [BMIm][BF_4]. Such metal nanoparticle deposits were not easy to remove from the Teflon surface by simple washing with organic solvents. The barely visible Rh-NP@stirring bar deposits (32 μg or less Rh metal,

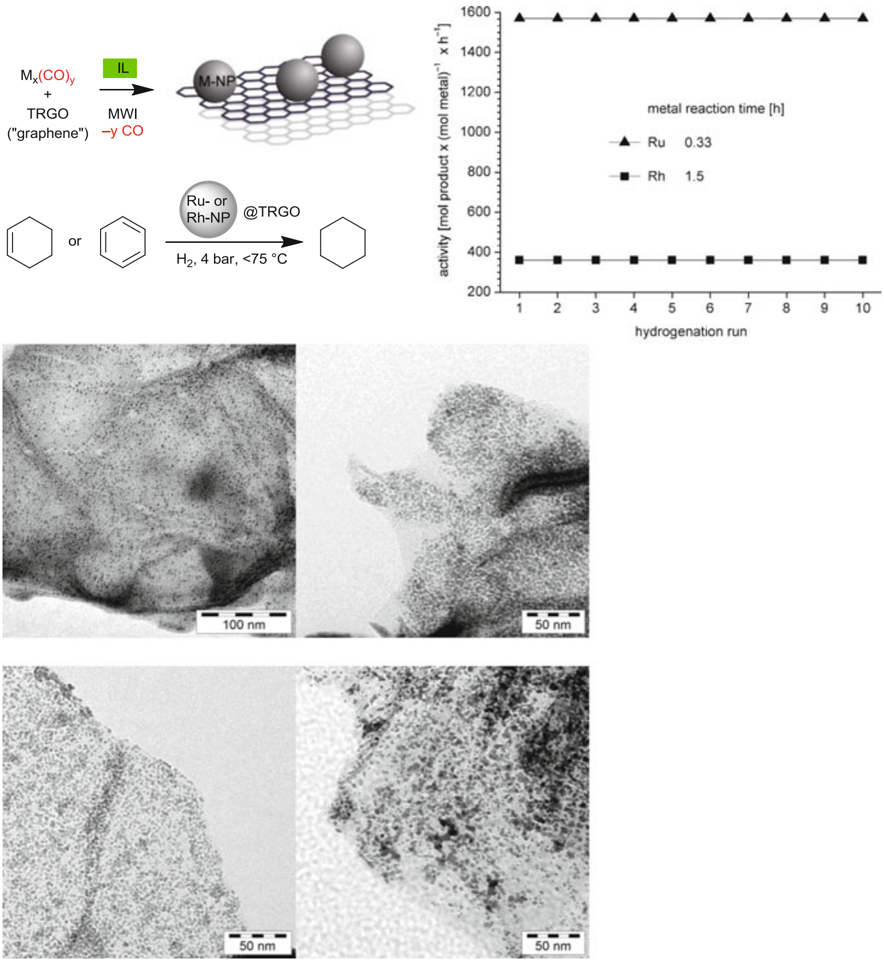

Fig. 19 Scheme for the synthesis of transition metal nanoparticles on thermally reduced graphite oxide (TRGO) in ILs by microwave treatment and the use of Ru- and Rh@TRGO for hydrogenation catalysis with activities for cyclohexene hydrogenation over 10 consecutive runs. TEM images *top row*: Ru-NP@TRGO before (*left*) and after (*right*) 10 hydrogenation runs; *bottom row*: Rh-NP@TRGO before (*left*) and after (*right*) 10 hydrogenation runs [175]. Reprinted in part from [175] with permission from the author; © 2010 Elsevier Ltd

Ø 2.1 ± 0.5 nm, on a 20 × 6 mm magnetic stirring bar) could act as an easy-to-handle and reusable catalyst in organic-solvent-free hydrogenation reactions with quantitative conversion and very high turnover frequencies of up to 32,800 mol cyclohexene × (mol Rh)$^{-1}$ × h^{-1} (Fig. 20) [178].

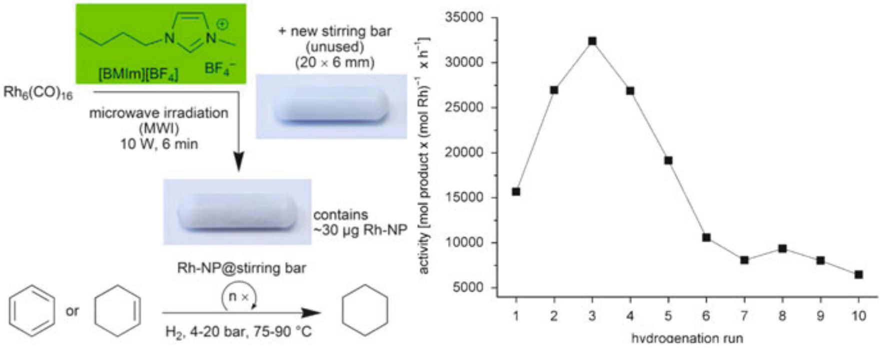

Fig. 20 Rh-NP deposition on a Teflon-coated magnetic stirring bar from an IL dispersion and the use of Rh-NP@stirring bar in hydrogenation catalysis with high activities [178]. Reprinted in part from [178] with permission from the author; © 2010 Elsevier Ltd

5 Conclusions

In this review, it is shown that ionic liquids are remarkable and excellent media for the synthesis and stabilization of metal nanoparticles (M-NPs) without the need of additional coordinating ligands, polymers, or surfactants. The stabilization of metal nanoparticles in ILs can be attributed to electrostatic and steric effects from the Coulomb network properties of ILs which prevent M-NP agglomeration. Various chemical synthesis methods of metal nanoparticles in ILs allow for the design of M-NP shapes and sizes. The synthesis of M-NPs can proceed by chemical, photochemical, sonochemical, and electroreduction as well as gas-phase deposition methods. A microwave-induced thermal decomposition of metal carbonyls $M_x(CO)_y$ in ILs provides an especially rapid and energy-saving access to M-NPs because of the significant absorption efficiency of ILs for microwave energy due to their high ionic charge, high polarity, and high dielectric constant. Metal carbonyls present attractive synthons for M-NPs as they are readily commercially available and contain the metal atoms already in the required zerovalent oxidation state needed. No reducing agent is necessary for metal carbonyls. The only side product is CO which is removed through the gas phase and avoids contaminations of the M-NP/IL dispersion. From the IL dispersion, the M-NPs can be deposited on various surfaces, such as nanotubes and thermally reduced graphite oxide (TRGO). The formation of bimetallic MM′-NPs in ILs has just been started, e.g., with intermetallic Cu/Zn-nanobrass and Ni/Ga nanoalloy phases. M-NP/IL dispersions have been successfully employed in organic-solvent-free catalytic reactions with multiple recycling of the M-NP catalyst.

Acknowledgment Our work was supported by the Deutsche Forschungsgemeinschaft through grant Ja466/17-1.

References

1. Yu S-H, MacGillivray LR, Janiak C (2012) CrystEngComm 14:7531–7534
2. Lu AH, Salabas EL, Schüth F (2007) Angew Chem Int Ed 46:1222–1244
3. Gedanken A (2004) Ultrason Sonochem 11:47–55
4. Rao CNR, Vivekchand SRC, Biswas K, Govindaraj A (2007) Dalton Trans 3728–3749
5. Mastai Y, Gedanken A (2004) In: Rao CNR, Müller A, Cheetham AK (eds) Chemistry of Nanomaterials, 1. Wiley-VCH, Weinheim, p 113
6. Park J, Joo J, Kwon SG, Jang Y, Hyeon T (2007) Angew Chem Int Ed 46:4630–4660
7. Peng Z, Yang H (2009) Nano Today 4:143–164
8. An K, Alayoglu S, Ewers T, Somorjai GA (2012) J Colloid Interface Sci 373:1–13
9. Kim M, Phan VN, Lee K (2012) CrystEngComm 14:7535–7548
10. Scholten JD, Leal BC, Dupont J (2012) ACS Catal 2:184–200
11. Yan N, Xiao C, Kou Y (2010) Coord Chem Rev 254:1179–1218
12. Pârvulescu VI, Hardacre C (2007) Chem Rev 107:2615–2665
13. Welther A, Jacobi von Wangelin A (2013) Curr Org Chem 17:326–335
14. Campbell PS, Prechtl MHG, Santini CC, Haumesser PH (2013) Curr Org Chem 17:414–429
15. Guerrero M, Than Chau NT, Noël S, Denicourt-Nowicki A, Hapiot F, Roucoux A, Monflier E, Philippot K (2013) Curr Org Chem 17:364–399
16. Scholten JD (2013) Curr Org Chem 17:348–363
17. Ostwald W (1901) Z Phys Chem 37:385
18. Ostwald W (1896) Lehrbuch der Allgemeinen Chemie, vol 2. Part 1. Wilhelm Engelmann, Leipzig
19. Bönnemann H, Richards RM (2001) Eur J Inorg Chem 2455–2480
20. Astruc D, Lu F, Aranzaes JR (2005) Angew Chem Int Ed 44:7852–7872
21. Pan C, Pelzer K, Philippot K, Chaudret B, Dassenoy F, Lecante P, Casanove M-J (2001) J Am Chem Soc 123:7584–7593
22. Aiken JD III, Finke RG (1999) J Am Chem Soc 121:8803–8810
23. Ueno K, Tokuda H, Watanabe M (2010) Phys Chem Chem Phys 12:1649–1658
24. Krämer J, Redel E, Thomann R, Janiak C (2008) Organometallics 27:1976–1978
25. Dupont J, Scholten JD (2010) Chem Soc Rev 39:1780–1804
26. Dupont J (2004) J Braz Chem Soc 15:341–350
27. Neouze M-A (2010) J Mater Chem 20:9593–9607
28. Consorti CS, Suarez PAZ, de Souza RF, Burrow RA, Farrar DH, Lough AJ, Loh W, da Silva LHM, Dupont J (2005) J Phys Chem B 109:4341–4349
29. Dupont J, Suarez PAZ, de Souza RF, Burrow RA, Kintzinger J-P (2000) Chem Eur J 6: 2377–2381
30. Vollmer C, Janiak C (2011) Coord Chem Rev 255:2039–2057
31. Janiak C (2013) Z Naturforsch B 68:1056–1089
32. Weingärtner H (2008) Angew Chem Int Ed 47:654–670
33. Xiao D, Rajian JR, Cady A, Li S, Bartsch RA, Quitevis EL (2007) J Phys Chem B 111: 4669–4677
34. Kuwabata S, Tsuda T, Torimoto T (2010) J Phys Chem Lett 1:3177–3188
35. Wasserscheid P, Keim W (2000) Angew Chem Int Ed 39:3772–3789
36. Krossing I, Slattery JM, Daguenet C, Dyson PJ, Oleinikova A, Weingärtner H (2006) J Am Chem Soc 128:13427–13434
37. Zhang H, Cui H (2009) Langmuir 25:2604–2612
38. Itoh H, Naka K, Chujo Y (2004) J Am Chem Soc 126:3026–3027
39. Kim K-S, Demberelnyamba D, Lee H (2004) Langmuir 20:556–560
40. Gao S, Zhang H, Wang X, Mai W, Peng C, Ge L (2005) Nanotechnology 16:1234–1237
41. Schrekker HS, Gelesky MA, Stracke MP, Schrekker CML, Machado G, Teixeira SR, Rubim JC, Dupont J (2007) J Colloid Interface Sci 316:189–195

42. Marcilla R, Mecerreyes D, Odriozola I, Pomposo JA, Rodriguez J, Zalakain I, Mondragon I (2007) Nano 2:169–173
43. Plechkova NV, Seddon KR (2008) Chem Soc Rev 37:123–150
44. Welton T (1999) Chem Rev 99:2071–2084
45. Feldmann C (2013) Z Naturforsch 68b 1057
46. Hallett JP, Welton T (2011) Chem Rev 111:3508–3576
47. Torimoto T, Tsuda T, Okazaki K, Kuwabata S (2010) Adv Mater 22:1196–1221
48. Janiak C (2013) Z Naturforsch 68b:1059–1089
49. Freudenmann D, Wolf S, Wolff M, Feldmann C (2011) Angew Chem Int Ed 50:11050–11060
50. Ahmed E, Breternitz J, Groh MF, Ruck M (2012) CrystEngComm 14:4874–4885
51. Ahmed E, Ruck M (2011) Dalton Trans 40:9347–9357
52. Groh MF, Müller U, Ahmed E, Rothenberger A, Ruck M (2013) Z Naturforsch 68b: 1108–1122
53. Morris RE (2009) Chem Commun 2990–2998
54. Parnham ER, Morris RE (2007) Acc Chem Res 40:1005–1013
55. Cooper ER, Andrews CD, Wheatley PS, Webb PB, Wormald P, Morris RE (2004) Nature 430:1012–1016
56. Rao CNR, Matte HSSR, Voggu R, Govindaraj A (2012) Dalton Trans 41:5089–5120
57. Lin Y, Dehnen S (2011) Inorg Chem 50:7913–7915
58. Lodge P (2008) Science 321:50
59. Verwey EJW, Overbeek JTG (1999) Theory of the stability of lyophobic colloids. Dover Publications Mineola, New York, pp 1–218
60. Redel E, Krämer J, Thomann R, Janiak C (2008) GIT Labor-Fachzeitschrift, GIT Verlag, Wiley-VCH Weinheim, April issue, 400–403
61. Shipway AN, Katz E, Willner I (2000) ChemPhysChem 1:18–25
62. Cassagneau T, Fendler JH (1999) J Phys Chem B 103:1789–1793
63. Keating CD, Kovaleski KK, Natan MJ (1998) J Phys Chem B 102:9404–9413
64. Kobrak MN, Li H (2010) Phys Chem Chem Phys 12:1922–1932
65. Schmid G (2010) Nanoparticles, 2nd edn. Wiley-VCH, Weinheim, pp 214–238
66. Branco LC, Rosa NJ, Ramos JJM, Alfonso CAM (2002) Chem Eur J 8:3671–3677
67. Yuan X, Yan N, Katsyuba SA, Zvereva E, Kou Y, Dyson PJ (2012) Phys Chem Chem Phys 14:6026–6033
68. Zhao D, Fei Z, Scopelliti R, Dyson P (2004) Inorg Chem 43:2197–2205
69. Zhao D, Fei Z, Geldbach TJ, Scopeliti R, Dyson P (2004) J Am Chem Soc 126:15876–15882
70. Prechtl MHG, Scholten JD, Dupont J (2009) J Mol Catal A 313:74–78
71. Fonseca GS, Umpierre AP, Fichtner PFP, Teixeira SR, Dupont J (2003) Chem Eur J 9: 3263–3269
72. Gelesky MA, Umpierre AP, Machado G, Correia RRB, Magno WC, Morais J, Ebeling G, Dupont J (2007) J Am Chem Soc 127:4588–4589
73. Dykeman RR, Yan N, Scopelliti R, Dyson PJ (2011) Inorg Chem 50:717–719
74. Dupont J, Fonseca GS, Umpierre AP, Fichtner PFP, Teixeira SR (2002) J Am Chem Soc 124:4228–4229
75. Fonseca GS, Machado G, Teixeira SR, Fecher GH, Morais J, Alves MCM, Dupont J (2006) J Colloid Interface Sci 301:193–204
76. Migowski P, Zanchet D, Machado G, Gelesky MA, Teixeira SR, Dupont J (2010) Phys Chem Chem Phys 12:6826–6833
77. Zhao X, Hua Y, Liang L, Liu C, Liao J, Xing W (2012) Int J Hydrogen Energy 37:51–58
78. Ruta M, Laurenczy G, Dyson PJ, Kiwi-Minsker L (2008) J Phys Chem C 112:17814–17819
79. Deshmukh RR, Rajagopal R, Srinivasan KV (2001) Chem Commun 1544–1545
80. Prechtl MHG, Scholten JD, Dupont J (2010) Molecules 15:3441–3461
81. Anderson K, Fernández SC, Hardacre C, Marr PC (2004) Inorg Chem Commun 7:73–76
82. Caló V, Nacci A, Monopoli A, Laera S, Cioffi N (2003) J Org Chem 68:2929–2933
83. Caló V, Nacci A, Monopoli A, Detomaso A, Iliade P (2003) Organometallics 22:4193–4197

84. Hassine F, Pucheault M, Vaultier M (2011) C R Chimie 14:671–679
85. Venkatesan R, Prechtl MHG, Scholten JD, Pezzi RP, Machado G, Dupont J (2011) J Mater Chem 21:3030–3036
86. Planellas M, Pleixats R, Shafir A (2012) Adv Synth Catal 354:651–662
87. Scheeren CW, Domingos JB, Machado G, Dupont J (2008) J Phys Chem C 112:16463–16469
88. Scheeren CW, Machado G, Dupont J, Fichtner PFP, Texeira SR (2003) Inorg Chem 42:4738–4742
89. Marquardt D, Barthel J, Braun M, Ganter C, Janiak C (2012) CrystEngComm 14:7607–7615
90. Raut D, Wankhede K, Vaidya V, Bhilare S, Darwatkar N, Deorukhkar A, Trivedi G, Salunkhe M (2009) Catal Commun 10:1240–1243
91. Gutel T, Garcia-Anton J, Pelzer K, Philippot K, Santini CC, Chauvin Y, Chaudret B, Basset J-M (2007) J Mater Chem 17:3290–3292
92. Setua P, Pramanik R, Sarkar S, Ghatak C, Rao VG, Sarkar N, Das SK (2011) J Mol Liq 162:33–37
93. Lazarus LL, Riche CT, Marin BC, Gupta M, Malmstadt N, Brutchey RL (2012) ACS Appl Mater Interfaces 4:3077–3083
94. Bhatt AI, Mechler A, Martin LL, Bond AM (2007) J Mater Chem 17:2241–2250
95. Dai T, Ge L, Guo R (2009) J Mater Res 24:333–341
96. Ryu HR, Sanchez L, Keul HA, Raj A, Bockstaller MR (2008) Angew Chem Int Ed 47: 7639–7643
97. Obliosca JM, Harvey I, Arellano J, Huang MH, Arco SD (2010) Mater Lett 64:1109–1112
98. Bai X, Li X, Zheng L (2010) Langmuir 26:12209–12214
99. Casal-Dujat L, Rodrigues M, Yagüe A, Calpena AC, Amabilino DB, González-Linares J, Borras M, Pérez-García L (2012) Langmuir 28:2368–2381
100. Lazarus LL, Yang AS-J, Chu S, Brutchey RL, Malmstadt N (2010) Lab Chip 10:3377–3379
101. Dash P, Miller SM, Scott RWJ (2010) J Mol Catal A Chem 329:86–95
102. Safavi A, Zeinali S (2010) Colloids Surfaces A Physicochem Eng Aspects 362:121–126
103. Li Z, Taubert A (2009) Molecules 14:4682–4688
104. Li Z, Friedrich A, Taubert A (2008) J Mater Chem 18:1008–1014
105. Khare V, Li Z, Mantion A, Ayi AA, Sonkaria S, Voelkl A, Thünemann AF, Taubert A (2010) J Mater Chem 20:1332–1339
106. Redel E, Walter M, Thomann R, Vollmer C, Hussein L, Scherer H, Krüger M, Janiak C (2009) Chem Eur J 15:10047–10059
107. Huang W, Chen S, Liu Y, Fu H, Wu G (2011) Nanotechnology 22:025602
108. Park H, Kim J-S, Choi BG, Jo SM, Kim DY, Hong WH, Jang S-Y (2010) Carbon 48: 1325–1330
109. Redel E, Walter M, Thomann R, Hussein L, Krüger M, Janiak C (2010) Chem Commun 46:1159–1161
110. Dinda E, Rashid MH, Biswas M, Mandal TK (2010) Langmuir 26:17568–17580
111. Marquardt D, Xie Z, Taubert A, Thomann R, Janiak C (2011) Dalton Trans 40:8290–8293
112. Taubert A (2010) Top Curr Chem 290:127–159
113. Liu D-P, Li G-D, Su Y, Chen J-S (2006) Angew Chem Int Ed 45:7370–7373
114. Taubert A, Li Z (2007) Dalton Trans 723–727
115. Redel E, Thomann R, Janiak C (2008) Inorg Chem 47:14–16
116. Ott LS, Finke RG (2006) Inorg Chem 45:8382–8393
117. Vollmer C, Redel E, Abu-Shandi K, Thomann R, Manyar H, Hardacre C, Janiak C (2010) Chem Eur J 16:3849–3858
118. Migowski P, Machado G, Teixeira SR, Alves MCM, Morais J, Traverse A, Dupont J (2007) Phys Chem Chem Phys 9:4814–4821
119. Zhu JM, Shen YH, Xie AJ, Qiu LG, Zhang Q, Zhang XY (2007) J Phys Chem C 111: 7629–7633
120. Firestone MA, Dietz ML, Seifert S, Trasobares S, Miller DJ, Zaluzec NJ (2005) Small 1: 754–760

121. Peppler K, Polleth M, Meiss S, Rohnke M, Janek J (2006) Z Phys Chem 220:1507–1527
122. Safavi A, Maleki N, Tajabadi F, Farjami E (2007) Electrochem Commun 9:1963–1968
123. Kim K, Lang C, Kohl PA (2005) J Electrochem Soc 152:E9
124. Redel E, Krämer J, Thomann R, Janiak C (2009) J Organomet Chem 694:1069–1075
125. Redel E, Thomann R, Janiak C (2008) Chem Commun 1789–1791
126. Salas G, Podgorsek A, Campbell PS, Santini CC, Pádua AAH, Costa Gomes MF, Philippot K, Chaudret B, Turmine M (2011) Phys Chem Chem Phys 13:13527–13536
127. Antonietti M, Kuang D, Smarly B, Zhou Y (2004) Angew Chem Int Ed 43:4988–4992
128. Scholten JD, Ebeling G, Dupont J (2007) Dalton Trans 5554–5560
129. Zhao L, Zhang C, Zhuo L, Zhang Y, Ying JY (2008) J Am Chem Soc 130:12586–12587
130. Guo S, Wang E (2007) Anal Chim Acta 598:181–192
131. Turkevich J, Stevenson PC, Hillier J (1951) Discuss Faraday Soc 11:55–75
132. Ryan TA, Ryan C, Seddon EA, Seddon KR (1996) Phosgene and related carbonyl halides, monograph 24. In: Clark RJH (ed) Topics in inorganic and general chemistry. Elsevier, Amsterdam, p 242
133. Mertens SFL, Vollmer C, Held A, Aguirre MH, Walter M, Janiak C, Wandlowski T (2011) Angew Chem Int Ed 50:9735–9738
134. Corma A, Domínguez I, Ródenas T, Sabater MJ (2008) J Catal 259:26–35
135. Miao S, Liu Z, Zhang Z, Han B, Miao Z, Ding K, An G (2007) J Phys Chem C 111: 2185–2190
136. Dash P, Scott RWJ (2011) Mater Lett 65:7–9
137. Marquardt D, Beckert F, Pennetreau F, Tölle F, Mülhaupt R, Riant O, Hermans S, Bartel J, Janiak C (2014) Carbon 66:285–294
138. Harada M, Kimura Y, Saijo K, Ogawa T, Isoda S (2009) J Colloid Interface Sci 339:373–381
139. Wang Z, Zhang Q, Kuehner D, Xu X, Ivaska A, Niu L (2008) Carbon 46:1687–1692
140. Endres F (2002) ChemPhysChem 3:144–154
141. Endres F, MacFarlane D, Abbott A (2008) Electrodeposition from ionic liquids. Wiley-VCH, Weinheim
142. Erb U (1994) US patent US 5,352,266
143. Natter H, Krajewski T, Hempelmann R (1996) Ber Bunsenges Phys Chem 100:55–64
144. Natter H, Hempelmann R (1996) J Phys Chem B 100:19525
145. Natter H, Schmelzer M, Löffler M-S, Krill CE, Fitch A, Hempelmann R (2000) J Phys Chem B 104:2467–2476
146. Przenioslo R, Wagner J, Natter H, Hempelmann R, Wagner W (2001) J Alloys Compounds 328:259–263
147. Natter H, Schmelzer M, Hempelmann R (1998) J Mater Res 13:1186–1197
148. Natter H, Bukowski M, Hempelmann R, Zein El Abedin S, Moustafa EM, Endres F (2006) Z Phys Chem 220:1275–1291
149. Cha J-H, Kim K-S, Choi S, Yeon S-H, Lee H, Lee C-S, Shim J-J (2007) Korean J Chem Eng 24:1089–1094
150. Yu L, Sun H, He J, Wang D, Jin X, Hu X, Chen GZ (2007) Electrochem Commun 9: 1374–1381
151. Zein El Abedin S, Endres F (2009) Electrochim Acta 54:5673–5677
152. Roy P, Lynch R, Schmuki P (2009) Electrochem Commun 11:1567–1570
153. Wei D, Baral JK, Österbacka R, Ivaska A (2008) J Mater Chem 18:1853–1857
154. Fu C, Kuang Y, Huang Z, Wang X, Du N, Chen J, Zhou H (2010) Chem Phys Lett 499: 250–253
155. Kareem TA, Kaliani AA (2012) Ionics 18:315–327
156. Suzuki T, Okazaki K-I, Suzuki S, Shibayama T, Kuwabata S, Torimoto T (2010) Chem Mater 22:5209–5215
157. Tsuda T, Yoshii K, Torimoto T, Kuwabata S (2010) J Power Sources 195:5980–5985
158. Hatakeyama Y, Takahashi S, Nishikawa K (2010) J Phys Chem C 114:11098–11102

159. Kameyama T, Ohno Y, Kurimoto T, Okazaki K-I, Uematsu T, Kuwabata S, Torimoto T (2010) Phys Chem Chem Phys 12:1804–1811
160. Wender H, de Oliveira LF, Migowski P, Feil AF, Lissner E, Prechtl MHG, Teixeira SR, Dupont J (2010) J Phys Chem C 114:11764–11768
161. Chen Q, Kaneko T, Hatakeyama R (2011) Curr Appl Phys 11:S63–S66
162. Kaneko T, Baba K, Hatakeyama R (2009) J Appl Phys 105:103306-1–103306-5
163. Xie Y-B, Liu C-J (2008) Plasma Processes Polym 5:239–245
164. Zein El Abedin S, Pölleth M, Meiss SA, Janek J, Endres F (2007) Green Chem 9:549–553
165. Brettholle M, Höfft O, Klarhöfer L, Mathes S, Maus-Friedrichs W, Zein El Abedin S, Krischok S, Janek J, Endres F (2010) Phys Chem Chem Phys 12:1750–1755
166. Meiss SA, Rohnke M, Kienle L, Zein El Abedin S, Endres F, Janek J (2007) ChemPhysChem 8:50–53
167. He P, Liu H, Li Z, Liu Y, Xu X, Li J (2004) Langmuir 20:10260–10267
168. Wei Z, Liu C-J (2011) Mater Lett 65:353–355
169. Aal AA, Al-Salman R, Al-Zoubi M, Borissenko N, Endres F, Höfft O, Prowald A, Zein El Abedin S (2011) Electrochim Acta 56:10295–10305
170. Richter K, Birkner A, Mudring A-V (2010) Angew Chem Int Ed 49:2431–2435
171. Tsuda T, Seino S, Kuwabata S (2009) Chem Commun 6792–6794
172. Imanishi A, Tamura M, Kuwabata S (2009) Chem Commun 1775–1777
173. Kerfoot DGE, Nickel X, Wildermuth E, Stark H, Friedrich G, Ebenhöch FL, Kühborth B, Silver J, Rituper R (2008) Iron compounds. In: Ullmann's encyclopaedia of industrial chemistry, 5th edn. Wiley-VCH, Weinheim
174. Hyeon T (2003) Chem Commun 927–934
175. Marquardt D, Vollmer C, Thomann R, Steurer P, Mülhaupt R, Redel E, Janiak C (2011) Carbon 49:1326–1332
176. Silva DO, Scholten JD, Gelesky MA, Teixeira SR, Dos Santos ACB, Souza-Aguiar EF, Dupont J (2008) ChemSusChem 1:291–294
177. Scariot M, Silva DO, Scholten JD, Machado G, Teixeira SR, Novak MA, Ebeling G, Dupont J (2008) Angew Chem Int Ed 47:9075–9078
178. Vollmer C, Schröder M, Thomann Y, Thomann R, Janiak C (2012) Appl Catal A 425–426: 178–183
179. Bogdal D (2006) Microwave-assisted organic synthesis. Elsevier, New York, pp 47–189
180. Buchachenko AL, Frankevich EL (1993) Chemical generation and reception of radio- and microwaves. Wiley-VCH, Weinheim, pp 41–56
181. Ahluwulia VK (2008) Alternative energy processes in chemical synthesis. Alpha Science International Ltd, Oxford
182. Berlan J, Giboreau P, Lefeuvre S, Marchand C (1991) Tetrahedron Lett 32:2363–2366
183. Langa F, de la Cruz P, de la Hoz A, Diaz-Ortiz A, Diez-Barra E (1997) Contemp Org Synth 4:373–386
184. Perreux L, Loupy A (2001) Tetrahedron 57:9199–9233
185. Stadler A, Kappe CO (2000) J Chem Soc Perkin Trans 2:1363–1368
186. Stadler A, Kappe CO (2001) Eur J Org Chem 919–924
187. Silveira ET, Umpierre AP, Rossi LM, Machado G, Morais J, Soares GV, Baumvol IJR, Teixeira SR, Fichtner RFP, Dupont J (2004) Chem Eur J 10:3734–3740
188. Gutel T, Santini CC, Philippot K, Padua A, Pelzer K, Chaudret B, Chauvin Y, Basset J-M (2009) J Mater Chem 19:3624–3631
189. Schütte K, Meyer H, Gemel C, Barthel J, Fischer RA, Janiak C (2014) Nanoscale in press. doi:10.1039/C3NR05780A
190. Langford JI, Wilson AJC (1978) J Appl Crystallogr 11:102–113
191. Campbell PS, Santini CC, Bouchu D, Fenet B, Philippot K, Chaudret B, Pádua AAH, Chauvin Y (2010) Phys Chem Chem Phys 12:4217–4223
192. Salas G, Santini CC, Philippot K, Collière V, Chaudret B, Fenet B, Fazzini PF (2011) Dalton Trans 40:4660–4668

193. Schütte K, Doddi A, Kroll C, Meyer H, Wiktor C, Gemel C, van Tendeloo G, Fischer RA, Janiak C (2014) Nanoscale submitted
194. Sawant AD, Raut DG, Darvatkar NB, Salunkhe MM (2011) Green Chem Lett Rev 4:41–54
195. Sheldon RA (2008) Chem Commun 3352–3365
196. Wasserscheid P, Welton T (2007) Ionic liquid in synthesis, vol 1. Wiley-VCH, Weinheim, pp 325–350
197. van Doorslaer C, Schellekens Y, Mertens P, Binnemanns K, De Vos D (2010) Phys Chem Chem Phys 12:1741–1749
198. Astruc D (2007) Nanoparticles and catalysis. Wiley-VCH, New York
199. Dupont J, de Souza RF, Suarez PAZ (2002) Chem Rev 102:3667–3692

Index